



저작자표시-비영리-변경금지 2.0 대한민국

이용자는 아래의 조건을 따르는 경우에 한하여 자유롭게

- 이 저작물을 복제, 배포, 전송, 전시, 공연 및 방송할 수 있습니다.

다음과 같은 조건을 따라야 합니다:



저작자표시. 귀하는 원저작자를 표시하여야 합니다.



비영리. 귀하는 이 저작물을 영리 목적으로 이용할 수 없습니다.



변경금지. 귀하는 이 저작물을 개작, 변형 또는 가공할 수 없습니다.

- 귀하는, 이 저작물의 재이용이나 배포의 경우, 이 저작물에 적용된 이용허락조건을 명확하게 나타내어야 합니다.
- 저작권자로부터 별도의 허가를 받으면 이러한 조건들은 적용되지 않습니다.

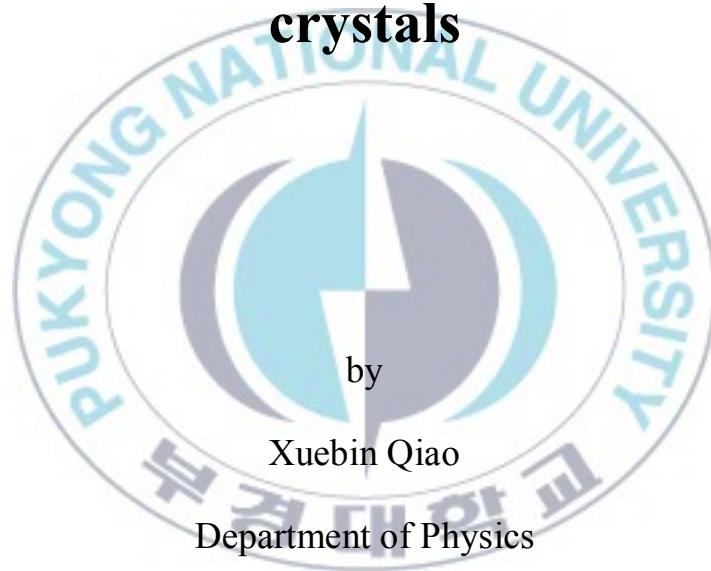
저작권법에 따른 이용자의 권리는 위의 내용에 의하여 영향을 받지 않습니다.

이것은 [이용허락규약\(Legal Code\)](#)을 이해하기 쉽게 요약한 것입니다.

[Disclaimer](#)

Thesis for the Degree of Master of Science

**Growth and luminescence properties
of Mn²⁺ ions doped in LiBaF₃ single
crystals**



by

Xuebin Qiao

Department of Physics

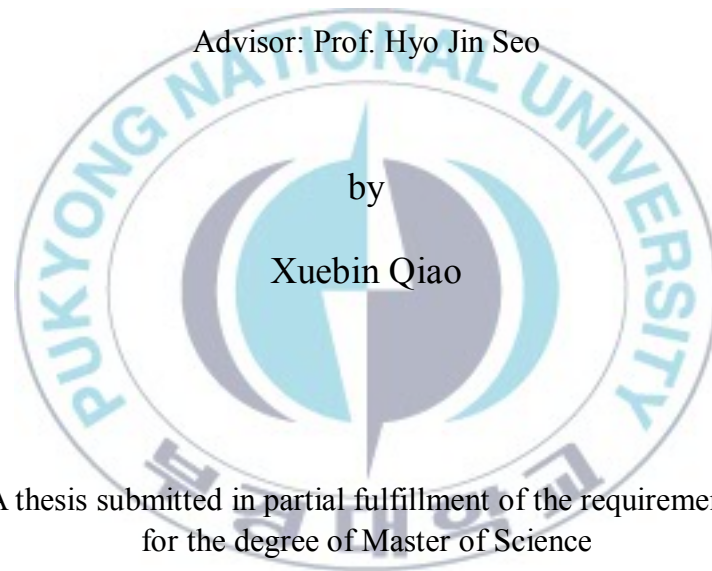
The Graduate School

Pukyong National University

August 2010

Growth and luminescence properties of Mn^{2+} ions doped in LiBaF_3 single crystals

Advisor: Prof. Hyo Jin Seo



by

Xuebin Qiao

A thesis submitted in partial fulfillment of the requirements
for the degree of Master of Science

In Department of Physics, The Graduate School,
Pukyong National University

August 2010

**Growth and luminescence properties of Mn²⁺ ions doped in
LiBaF₃ single crystals**

A dissertation

by

Xuebin Qiao

Approved by:

Prof. Jae Yong Je (Chairman)

Dr. Kyoung Hyuk Jang (Member)

Prof. Hyo Jin Seo (Member)

August 25, 2010



Contents

Abstract	iii
1. Introduction	1
2. Theoretical background	3
2.1 Light interactions with solids	3
2.2 Luminescence, fluorescence and photoluminescence	4
2.3 Absorption	10
2.4 Emission	13
2.5 Photoluminescence properties of Mn^{2+}	16
2.6 $LiBaF_3$ crystal structure	21
2.7 Point defects in crystals	24
2.8 Calculation of lifetime	25
3. Experimental	27
3.1 Crystal growth by Czochralski method	27
3.2 Growth procedure of the $LiBaF_3$ single crystal	29
3.2.1 Synthesis of $LiBaF_3$ precursor powder	29
3.2.2 Crystal growth of $LiBaF_3$ single crystals	31
3.2.3 Sample machining	34

3.2.4 Several factors influencing the crystal growth.....	36
3.2.4.1 The initial temperature cooling rate.....	36
3.2.4.2 Rotation and pulling speed	36
3.3 Fluorescence dynamics spectrometer.....	37
3.4 Crystal structure characterization	39
3.5 Luminescence spectrometer.....	40
3.6 Absorption spectrometer.....	41
4. Results and discussion	42
4.1 X-ray diffraction analyze	41
4.2 Fluorescence Testing results	44
4.2.1 Absorption spectra	44
4.2.2 Mn-related Complex.....	46
4.2.2.1 Band A - green emission.....	49
4.2.2.2 Band B- near IR emission	60
5. Conclusion	67
References	69

Growth and luminescence properties of Mn²⁺ ions doped in LiBaF₃ single crystals

Xuebin Qiao

Department of Physics
Pukyong National University

Abstract

The manganese doped LiBaF₃ single crystals were grown by the Czochralski method. The conditions of preparation and growth of manganese doped LiBaF₃ were investigated. The different concentrations of Mn-doped powder were checked by XRD. The reaction conditions were investigated to get pure LiBaF₃ powder. The Mn²⁺ ion substitutes for Ba²⁺ ion or the Li⁺ ion in the LiBaF₃ crystal. The emission spectra showed the 3d-3d band emission peak at 515 nm when Mn²⁺ is substituted into the Ba²⁺ in the cubic crystalline field. Another band emission peak was found centered at 750 nm which could be ascribed to 3d-3d emission of Mn²⁺ when it substitutes for Li⁺ in the octahedral crystal field. The spectra of Mn²⁺-doped crystals with different concentrations were compared. The luminescent lifetime of 515 nm and 750 nm emissions were measured under different temperatures. The lifetime curves show the temperature quenching of ⁴T₁-⁶A₁ emission level. The zero-phonon lines of the 3d-3d transition in two kinds of sites were observed at the low temperature.

1. Introduction

$AMeF_3$ perovskites, where A is an alkali metal, Me is a transition metal, and F is a fluorine ion were known to have the same type of crystal structure as $CaTiO_3$. These compounds doped with an activator ion, e.g. Mn^{2+} , are known to emit an enhanced luminescence after irradiation. This was first observed by Sibley and Koumvakalis in $RbMgF_3:Mn^{2+}$ [1]. It was supposed that an F-centre (electron trapped at an anion vacancy), in the vicinity of the Mn dopant, enhances the oscillator strength leading to increased emission intensity. A similar effect was observed in $RbCdF_3:Mn^{2+}$, where after x-irradiation an increased luminescence and an additional absorption band around 310 nm occurs; this band can also be observed in nominally pure $RbCdF_3$ [2]. The 310 nm band was tentatively assigned to intrinsic defects being created upon x-irradiation. The radiation-induced luminescence intensity is correlated with the x-ray dose; Mn-doped $RbCdF_3$ has potential as a radiation dosimeter material.

$LiBaF_3$ crystal is also known as a scintillation material. It has been applied in vacuum ultraviolet optical lithography, X-ray storage phosphor and other luminescent devices [3-5]. This inorganic material is remarkable because of the presence of both core valence luminescence (CV) and self

trapped-exciton luminescence (STE) under gamma irradiation whereas only the STE luminescence is present under neutron or alpha-irradiation, which makes it suitable for applications as a thermal neutron detector [6]. The CV luminescence is found between 190 and 220 nm. This is a basis to developing fast scintillators. However, the presence of oxygen impurities is a restricting factor for this usage [7], which changes the sensitivity of this material to ionizing radiation and optical properties.

The experiments on pure and oxygen doped LiBaF_3 crystal have been performed by Shiran et al. [8]. For oxygen doped crystal, there exhibits some new absorption bands in the region of 208–280 nm in the UV part of the spectrum. The presence of new absorption bands may be related to the impurity oxygen ions. In the process of crystal growth, it is found that oxygen ions are easily incorporated into the crystal and enhance the absorption band in 180–230 nm range [9]. The O: LiBaF_3 crystal has attracted extensive attention, because additional absorption bands are overlapped with the useful fast core-valence luminescence, resulting in a decrease in the light yield. In an earlier study on the structures of oxygen-doped BaFCl and BaF_2 by photoluminescence-detected electron paramagnetic resonance [10, 11], it is claimed that the oxygen may substitute for fluorine and combine with a next nearest fluorine vacancy forming the defect cluster $[\text{O}'_{\text{F}} + \text{V}'_{\text{F}}]$ in the crystal.

The Czochralski process is a method of crystal growth used to obtain single crystals of semiconductors (e.g), metals (e.g. palladium, platinum, silver, gold), salts and many oxide crystals (LaAlO₃, YAG, .and GGG etc). The process is named after Jan Czochralski, who discovered the method in 1916 while investigating the crystallization rates of metals.

In this work we present optically stimulated luminescence material: Mn-doped LiBaF₃. Single crystal LiBaF₃ with 0.05mol% and 0.5mol% Mn²⁺ were prepared by the Czochralski method. The photoluminescence spectra and decay time under different excitation regions, as well as different temperatures are available in this paper. As you know Luminescence of Mn²⁺ ions doped inorganic compounds usually gives broad band emission. The wavelength position of the emission bands depends strongly on the host lattice. So this experimental objective is to investigate the crystal field which depends on the host structure by analyze the luminescence properties of Mn²⁺.

2. Theoretical background

2.1 Light interactions with solids

If a solid sample is illuminated by a light beam of certain intensity, in

general, the intensity of the transmitted beam is lower than that of the incident beam. Several processes can contribute to this attenuation such as:

- Absorption, if the beam frequency is resonant with a ground to excited state transition of the atoms in the solid. A fraction of this intensity is generally emitted at a lower frequency than that of the incident beam, giving rise to the emission intensity. The remnant of the absorbed intensity is lost through nonradiative processes (heat).
- Reflection with a different intensity from the external and internal surfaces.
- Scattering, with a light spread in several directions, due to elastic (at the same frequency as the incident beam) or inelastic (at lower and higher frequencies than that of the incident beam – Raman scattering) processes.

Optical spectroscopy analyzes frequencies and intensities of these emerging beams as a function of frequency and intensity of the incident beam.

2.2 Luminescence, fluorescence and photoluminescence

The word luminescence, including both fluorescence and phosphorescence, originates from the Latin word lumen, which means light. In spectroscopy the word luminescence is defined as a phenomenon in which the electronic state of a substance is excited by external energy stimulus and the excitation energy is given off as light. Here, the light includes not only electromagnetic waves in the visible region of 400 to 750 nm, but also those in the neighboring regions on both ends, i.e., near-ultraviolet (UV) and near infrared (IR) regions [12].

The visible light emission from a substance during the time when it is exposed to exciting radiation is called fluorescence, while the after-glow if detectable by the human eye after the cessation of excitation is called phosphorescence. In excited singlet states, the electron in the excited orbital is paired (by opposite spin) to the second electron in the ground-state orbital. Consequently, return to the ground state is spin allowed and occurs rapidly by emission of a photon. The typical fluorescence lifetime is near 10 ns (10×10^{-9} s) [13].

Phosphorescence is the emission of light from triplet-excited states, in which an electron in the excited orbital has the same spin orientation as the ground-state electron. Transitions to the ground state are forbidden and the emission rates are slow so that phosphorescence lifetimes are typically milliseconds to seconds [14].

Photoluminescence occurs after excitation with light (i.e., radiation within the optical range). Luminescence can also be produced under excitation with an electron beam, and in this case it is called cathodoluminescence. This technique is conventionally used to investigate some characteristics of specimens, such as trace impurities and lattice defects, as well as to investigate crystal distortion. Excitation by high-energy electromagnetic radiation (sometimes called ionizing radiation) such as X-rays, α -rays (helium nuclei), β -rays (electrons), or γ -rays leads to a type of photoluminescence called radioluminescence [15]. Fig 2.1 provides the classification of the different types of luminescence.

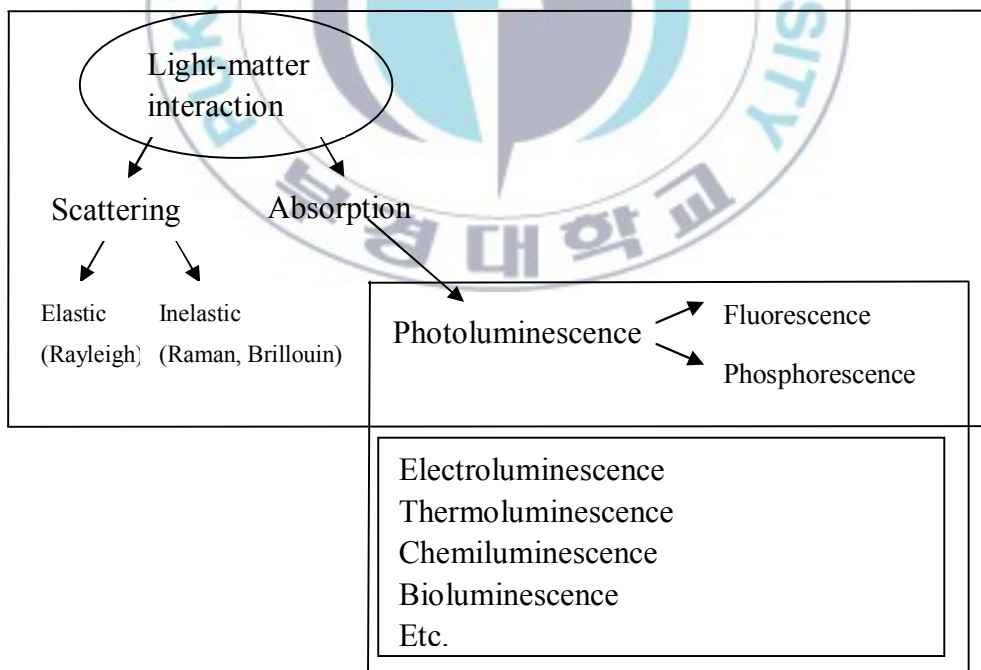


Fig. 2.1 Various types of luminescence with corresponding excitation [15]

Fluorescence occurs when an atom, molecule or solid absorbs light photons from the UV visible light spectrum, known as excitation, and then rapidly emits light photons as it returns to its ground state; the state of lowest energy of that electron, thus it is given more energy and convert to a higher electronic energy state what is called “excited state”. In the excited state, an electron will not stay there too long since it is not stable, then the electron gives back the energy in the form of light and return to its ground state [16].

Fluorimetry characterizes the relationship between absorbed and emitted photons at specified wavelengths. It is a precise, quantitative, and analytical technique that is inexpensive and easily mastered. All chemical compounds absorb energy which causes excitation of electrons bound in the molecule, such as increased vibrational energy or, under appropriate conditions, transitions between discrete electronic energy states. For a transition to occur, the absorbed energy must be equivalent to the difference between the initial electronic state and a high-energy state. This value is constant and characteristic of the molecular structure. This is termed the excitation wavelength. If conditions permit, an excited molecule will return to its ground state by emission of energy through heat and/or emission of energy quanta such as photons.

Fluorescent compounds or fluorophores can be identified and quantified on the basis of their excitation and emission properties. The excitation spectra are determined by measuring the emission intensity at a fixed wavelength, while varying the excitation wavelength. The emission spectra are determined by measuring the variation in emission intensity wavelength for a fixed excitation wavelength [13].

During the excited-state lifetime, typically 1-10 nanoseconds, the fluorophore energy S_1' is dissipated and converts to a lower energy excited state S_1 where fluorescence emission originates. That means not all absorbed energy converts to fluorescence emission when electrons return to ground state [16]. The vibrational energy loss results in an emission spectrum with longer wavelengths compared to the absorption/excitation spectrum is represented by $C(h\nu_{ex} - h\nu_{em})$ which is known as Stokes shift, where h is Planck's constant and ν is the frequency of light. Therefore emitted photons have longer wavelengths than excited photons.

If S_1' denotes an excited state of a substance S_0 , then fluorescence consists of the excitation: $S_0 + h\nu_{ex} \rightarrow S_1'$ and emission: $S_1 \rightarrow h\nu_{em} + S_0$. Generally speaking, the absorbed photon is in the UV range, and the emitted light is in the visible range.

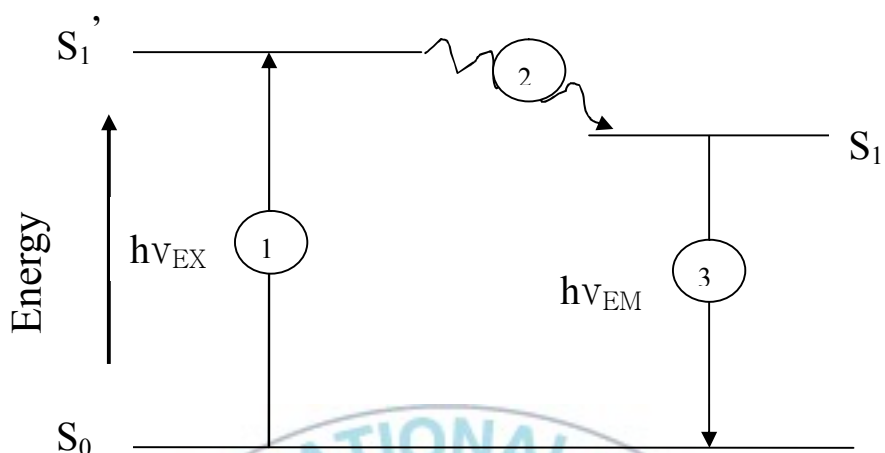


Fig. 2.2 A diagram illustrating the processes of excitation and emission of fluorescence.

Quantum yield is the percentage of molecules in an excited electronic state that decay to ground state by fluorescent emission, i.e., rapid emission of a light photon in the range of 200- 900 nm. This value is always less than or equal to unity and is characteristic of the molecular structure.

Several factors contribute to the decay of the fluorophores and thus, reduce the fluorescence intensity and the quantum yield. In general, decay processes can be classified as: internal or external conversions [17]. Internal conversion is a process at which the electron energy is converted to vibrational energy of the fluorophore itself. Since vibrational processes are driven by thermal processes, the internal conversion rate typically increases

with temperature, which accounts for the commonly observed decrease in fluorescence intensity with rising temperature. External conversion describes the process where the fluorophore loses electronic energy to its environment through collision with other solutes. Upon collision, the fluorophore is deexcited nonradiatively. A number of important solute ions, such as oxygen, are efficient fluorescence quenchers. Usually, a fluorophore can be chemically bound to a quencher to form a 'dark complex' – a product that does not fluoresce [17].

2.3 Absorption

Luminescent materials only emit radiation when the excitation energy is absorbed. Excitation spectra and absorption spectra typically show a strong correlation and both indicate that excitation energy can be absorbed either by the host lattice or by the activator itself. When high energy excitation such as fast electrons, gamma rays or X-rays and in our case, vacuum ultraviolet radiation is used, this always results in host lattice excitation. On the other hand, direct excitation of the activator is only possible with near-ultraviolet or visible radiation. The excitation spectra can tell us whether the host lattice or the activator absorbs the incident radiation.

The optical properties of a particular luminescent center in different host lattices are usually different because the immediate surroundings of such a

center have been changed. Two main factors can be said to be responsible for the influence of the host lattice on the optical properties of a given activator in different host lattices. The first factor is covalency and the other is the crystal field. For higher covalency, the host lattice interactions between the electrons are reduced because they spread out over wider orbitals. Hence electronic transitions between different energy levels, which are determined by electron interaction shift to lower energy. A higher covalency also means that the constituent ions have a lower electronegativity difference between them so that the charge transfer transitions between these ions also shift to lower energy. For example, because YF_3 is more ionic than Y_2O_3 , the charge transfer absorption band of Eu^{3+} shifts to a lower energy in the more covalent Y_2O_3 [18]. Based on this, we can assume that Sr substitution for Ca would yield a more covalent compound and cause the excitation band to move to a lower energy or higher wavelength. Conversely, alloying with Zn would move the excitation band to higher energies, which is would be consistent with our goal of shifting to lower excitation wavelengths. Ta has approximately the same electronegativity as Nb and so it is difficult to judge this effect in the metaniobate alloy system.

The effect of the crystal field effect of the host lattice on the optical properties of a luminescent ion is the second factor that influences the properties of an activator. The crystal field is the electric field imposed on the

ion due to its surroundings. The strength of the crystal field then determines the spectral position of certain optical transitions. Different host lattices yield different crystal fields, which in turn yield different splittings such that the luminescent center can serve as a probe of the surroundings. Thus, the crystal field is responsible for the splitting of certain optical transitions and these observed splittings yield site symmetry.

One visible effect of the host lattice is the inhomogeneous broadening of the spectra. In powders, for example, the external surface may be large and activator ions, such as Eu^{3+} , near the surface may experience a covalency and a crystal field that is different from the bulk. These ions therefore have their optical transitions at slightly different energies from those in the bulk, which causes the spectra to broaden. Point defects in the crystal structure also contribute to this broadening. This effect helps to explain why even though calcium metaniobate is highly crystalline; we see a broad host absorption band. This broad band is also due to the vibrational overlap that occurs as a result of the interaction between the optical center and the vibrations of its surroundings. Vibrational overlap with several levels results in a broader absorption band and the larger the difference in chemical bonding between the excited state and the ground state, the broader the absorption band [18]. The excited state in the NbO_6 complex of CaNb_2O_6 consists of Nb^{5+} ions and the valence state consists of O^{2-} ions. The bond enthalpy of the Nb-O bond is 771.5 KJ/mol, which is much higher

than the Nb-Nb bond enthalpy (510 KJ/mol), when compared to the Nb-C bond enthalpy and most other bond enthalpies with Nb. Thus, the vibrational overlap contribution to band broadening can also be accounted for in CaNb_2O_6 .

2.4 Emission

Emission can be defined as a radiative return to the ground state. Such a radiative return can occur when the absorption and emission processes occur in the same luminescent ion or center, or it can occur as a result of the influence of the host lattice on the emission transitions.

Typically, there is little or no emission during the relaxation process. The system can then return to the ground state upon the emission of radiation. This emission occurs spontaneously in the absence of a radiation field, while absorption can only occur in the presence of a radiation field. Emission in the presence of a radiation field is known as stimulated emission, but this process is not within the scope of this thesis. After emission, the luminescent center reaches a high vibrational level of the ground state, from which it relaxes to the lowest vibrational level of the ground state. The energy difference between the maximum of the excitation band and that of the emission band is known as the Stokes' shift. The larger

the vibrational overlap, the larger the Stokes' shift and the broader the optical bands.

Energy transfer can occur between a pair of dissimilar luminescent centers or between identical luminescent centers. The case of dissimilar luminescent centers involves two centers: a sensitizer S and an activator A separated in a solid by a distance R, where R is assumed to be so short that S and A have a non-vanishing interaction with one another. This means that if S is in an excited state while A is in the ground state, then the relaxed excited state of S may transfer its energy to A. In this case, resonance has to be satisfied, that is, the energy differences between the ground and excited states have to be equal and a suitable interaction has to exist for energy transfer to occur. This interaction can be an exchange interaction where there is a wave function overlap or an electric or magnetic multipolar interaction [18].

Energy transfer between identical luminescent centers results in the phenomenon of concentration quenching of luminescence and a weak-coupling scheme or strong coupling scheme can be applied to these centers. A typical case of stronger coupling is well-known in groups like tungstates and vanadates, which are oxidic anions with a central metal ion which has no d electrons, e.g. WO_4^{2-} , WO_6^{6-} , VO_4^{3-} and MoO_4^{2-} . Because the Stokes' shift of their emission is usually very large ($\sim 16000\text{cm}^{-1}$), energy

migration is completely hampered, even at room temperature, e.g. in CaWO_4 . In other cases such as YVO_4 , thermally activated energy migration occurs and the Stokes' shift is much smaller ($\sim 10,000\text{cm}^{-1}$). The luminescent groups in WO_4^{2-} and NbO_4^{3-} have been proven to be isolated luminescent centers in spite of the short distance to their nearest neighbors [18]. The nature of the luminescent species determines the strength of the electron lattice coupling, for example, in the weak coupling case, the zero phonon line dominates and we see narrow peaks as in a Eu^{3+} emission. The coupling can be intermediate, in which case there is a gradual progression in the symmetrical stretching mode and where there is a broad band, this is an indication of strong coupling such as in CaNb_2O_6 .

Transition metal ion complexes with a formally empty d shell typically show intense broad-band emission with a large Stokes shift on the order of 10000cm^{-1} - 20000cm^{-1} . Examples are VO_4^{3-} , NbO_6^{7-} , WO_4^{2-} and WO_6^{6-} . In the excited state, the electronic charge has moved from the oxygen ligands to the central metal ion and this is considered to be a charge transfer state. Actually, the amount of charge transfer is normally small but a significant amount of electronic reorganization occurs whereby electrons are promoted from bonding orbitals in the ground state to antibonding orbitals in the excited state. This leads to a large value of ΔR in the configurational coordinate diagram, and broad spectral bands [18]. As can be expected, in CaNb_2O_6 , where the electrons are promoted from O^{2-} bonding orbitals in the

ground state, to the Nb^{5+} antibonding orbitals in the excited state, consequently the Stokes shift is large and the spectral bands are broad. In addition, the complexes with lighter metal ions, such as $\text{Mg}_4\text{Nb}_2\text{O}_9$, YVO_4 , CaWO_4 and probably CaNb_2O_6 , show long decay times as it has been proven that the emitting state in such compounds is a spin triplet [19].

2.5 Photoluminescence properties of Mn^{2+}

Luminescence of Mn^{2+} ions doped inorganic compounds usually gives broad band emission. The lifetime of Mn^{2+} luminescence is of the order of millisecond. The wavelength position of the emission bands depends strongly on the host lattice. From the Tanabe–Sugano diagram, the emission corresponds to the ${}^4\text{T}_1 \rightarrow {}^6\text{A}_1$ transition of Mn^{2+} ions can varies in a wide range in the entire spectral wavelength [20]. For example, the tetrahedrally coordinated Mn^{2+} (weak crystal-field) usually gives a green emission, whereas octahedrally coordinated Mn^{2+} (strong crystal-field) gives an orange to red emission [21]. In the following section the electronic structure of Mn^{2+} will be explained in order to understand the optical properties. Mn^{2+} has an incompletely filled d shell and its electron configuration is d^5 . The energy levels originating from this configuration have been calculated by Tanabe and Sugano considering the interaction between the d electrons and the crystal field [19].

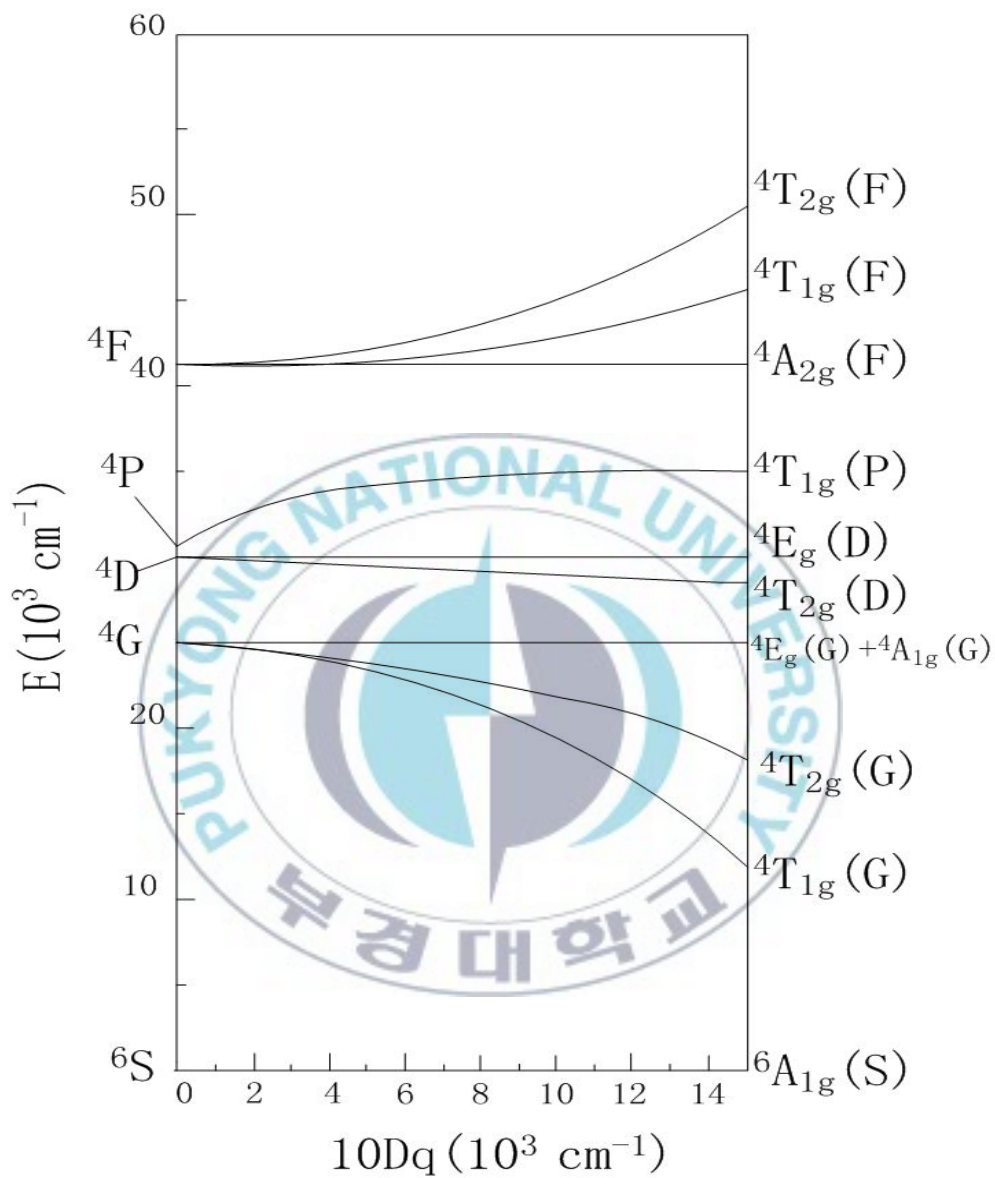


Fig. 2.3 The energy levels of Mn^{2+} as a function of the octahedral crystal field ($10Dq$). The x axis represents the ground state.

The energy levels of a free ion can be found on the left hand side of this Tanabe-Sugano diagram. Many of these levels split into more sub-levels if a crystal field $10Dq \neq 0$. The ground state is represented by the x axis. The free ion levels are marked ^{2S+1}L , where S presents the total spin quantum number, and L the total orbital angular momentum. The degeneracy of these levels is $2L+1$ and can be lifted by the crystal field. Crystal field energy levels are marked ^{2S+1}X , where X may be A for no degeneracy, E for a twofold degeneracy and T for a threefold degeneracy. Subscripts indicate certain symmetry properties and the letter in brackets represents the energy level of the free ion. For further information the reader is referred to other reference [19, 22].

The Tanabe-Sugano diagram for Mn^{2+} in an octahedral O_h surrounding is shown in figure 2.3. The ground state is $^6A_{1g}(S)$. Since these energy levels are all within the d shell, all transitions from the ground state to excited levels are spin and parity forbidden. However, the Mn^{2+} transitions can still be observed. It was suggested that the selection rule is relaxed through a spin-spin interaction and a vibronic mechanism, where the electronic transitions are coupled with vibrations of suitable symmetry [22].

Exciting a system with UV light brings an electron of Mn^{2+} in a high vibrational level of the excited state, as shown in figure 2.4. The electron

falls to the lowest vibrational level of the excited state giving up the excess energy to the surrounding. Another way to describe this process is to say that the nucleus adjusts its position to the excited state, so the interatomic distance varies from the distance it has in equilibrium. The configurational coordinate changes by ΔR . This process is called relaxation. From the lowest vibrational level the electron can return to the ground state spontaneously under emission of radiation. It can be seen that the emission has a lower energy than the excitation of the same excited level. This effect is called Stokes Shift.

Since the crystal field strength varies during the vibration the Tanabe-Sugano diagram predicts the width of the band. If the level runs parallel to the ground level, a variation of ΔR will not influence the transition energy and a narrow band can be expected. If the excited level has a slope relative to the ground state, a variation of ΔR will influence the transition energy, and a broad transition band can be expected. Because of this, the ${}^4T_{1g}(G)$ is most sensitive to changes in ΔR and has significant different values for all systems. Therefore it is easy to explain why the wavelength position of the emission bands of Mn^{2+} depends strongly on the host lattice.

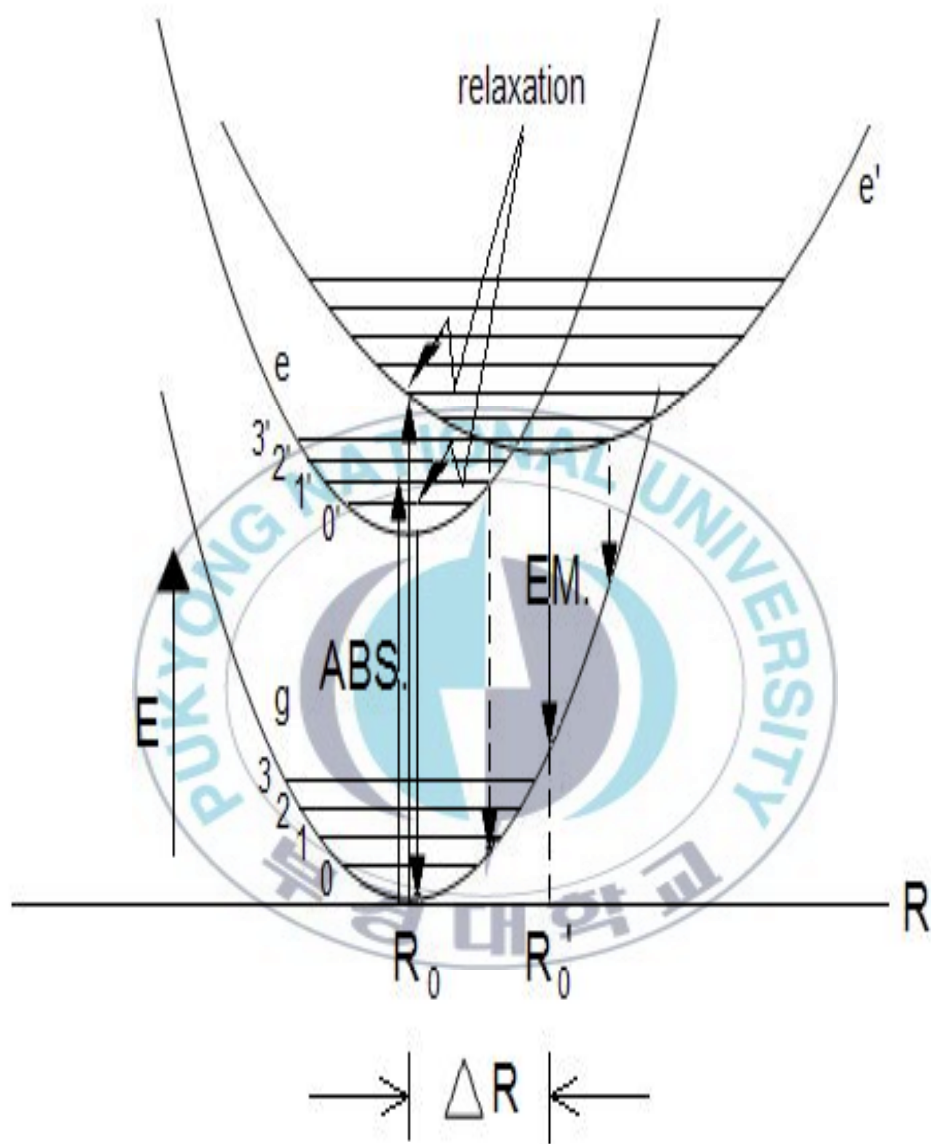


Fig. 2.4 Configurational coordinate diagram. After absorption the system reaches a high vibrational level of the excited state. Subsequently it relaxes to the lowest vibrational level from where the emission occurs.

2.6 LiBaF₃ crystal structure

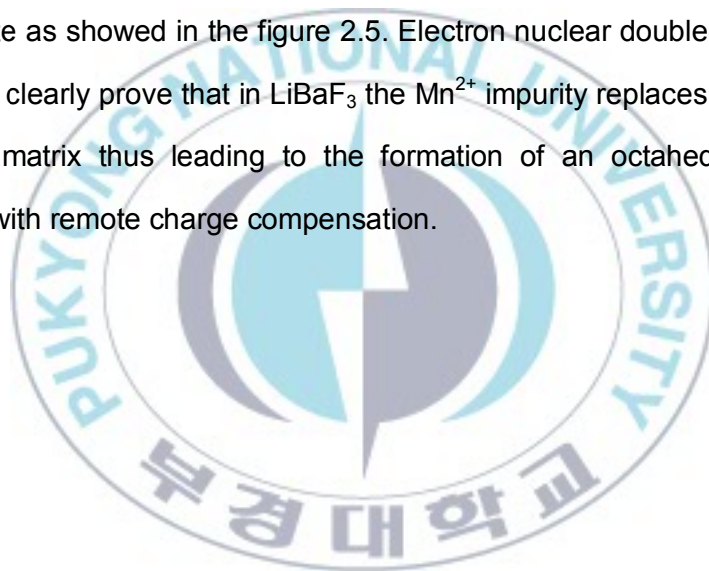
The name perovskite represents a group of crystals having the same structure. The perovskites presented in this work have an AMeF₃ structure, where A stands for a cation, Me for a metal and F for fluorine. The crystal structure of AMeF₃ perovskites depends on the tolerance factor *t*, which gives a relation between the radii of the cation, the metal, and the fluorine. The tolerance factor is defined by

$$t = \frac{r_A + r_F}{\sqrt{2}(r_{Me} + r_F)} \quad (2.1)$$

A perovskite structure is expected if *t* has a value within the range $0.76 \leq t \leq 1.13$. The ideal cubic structure of AMeF₃ belongs to a tolerance factor range of $0.88 \leq t \leq 1.00$, space group Pm3m. The A-ions have 12 fluorine neighbors while the metal ions have six. Thus, the metal ions with six neighbors form a MeF₆ octahedron, which is linked to a neighboring MeF₆ octahedron by sharing the corners throughout the structure.

Crystalline LiBaF₃ is a typical ABF₃ material (herein A-alkali ion, B-alkali-earth ion, X-halide ion) which has inverse-perovskite with cubic structure ($a_0 = 3.988 \text{ \AA}$) [23]. Lithium has an oxidation state of +1 ($r = 0.76 \text{ \AA}$,

CN=6) and barium of +2 (1.61 Å, CN=12) [24], where the tolerance factor is 0.94. Since LiBaF_3 has a tolerance factor of 0.94, it has a cubic perovskite structure. It has no distortions even at low temperatures [25]. The monovalent Li^+ ion is surrounded by 6 fluorines and Ba^{2+} is surrounded by 12 fluorines. Although Mn^{2+} has the same charge as Ba^{2+} it does not substitute for the Ba ion. Yosida [18] showed that the Mn^{2+} ion substitutes for the Li^+ ion, which is surrounded by a fluorine octahedron. Mn^{2+} is located on the Me site as showed in the figure 2.5. Electron nuclear double-resonance (ENDOR) clearly prove that in LiBaF_3 the Mn^{2+} impurity replaces a Li^+ ion of the host matrix thus leading to the formation of an octahedral MnF_6^{4-} complex with remote charge compensation.



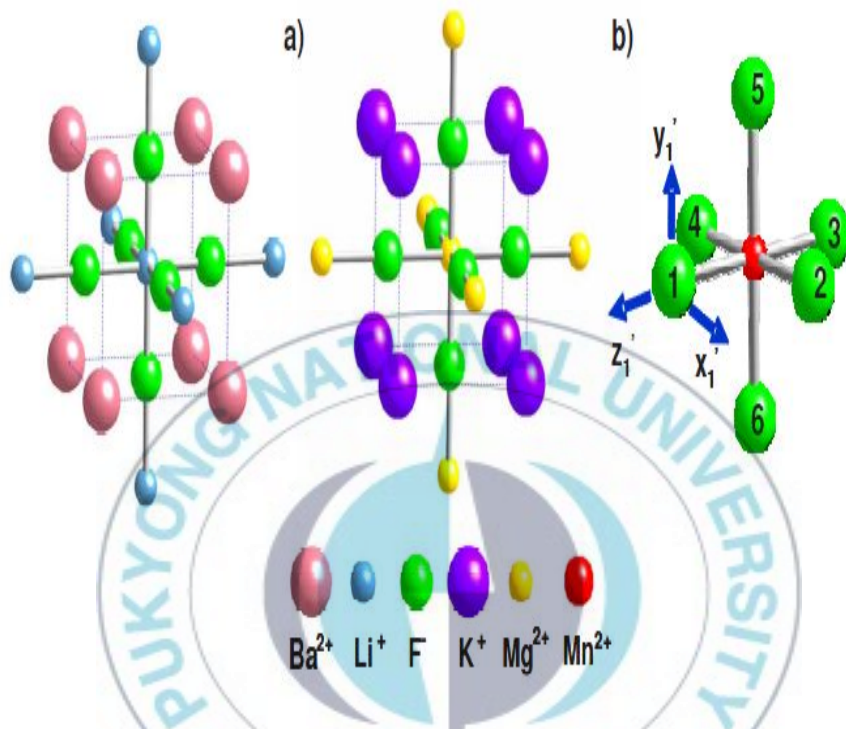


Fig. 2.5 (Color online) a) 21 atom clusters used in the calculations of the inverted LiBaF₃ (left) and normal KMgF₃ (right) perovskite structures. Unit cells are marked with dashed lines. The lattice constant (a) is thus equal to 2R₀. Similar clusters were used for the calculations of the corresponding Mn²⁺ impurity centers but replacing the central ion (Li⁺ in LiBaF₃ and Mg²⁺ in KMgF₃) by Mn²⁺. B) MnF₆⁴⁻ complex and arrangement of local axes for ligand 1 placed on the x axis.

Another property in perovskite systems is the distance between the Me and the F ions R_{MeF} . The 10Dq parameter strongly depends on RMF by the inverse power law found by Rodriguez [26]. They showed that the dependence of 10Dq with R_{MeF} can be described in the form

$$10Dq = K \cdot R_{\text{MeF}}^{-n} \quad (2.2)$$

where K and n are constants. However, this law is only valid in a small range of R_{MeF} (2.0-2.2 Å).

2.7 Point defects in crystals

There are many different types of point defects in crystals. The simplest defect is an anion vacancy, which has an effective positive charge. When an electron is trapped by this vacancy, this defect is called an F-centre. Since this electron experiences a potential, it has a specific absorption spectrum, comparable to a H-atom. Other, so-called, colour centres are created as complexes of this simple defect. If there are n F-centres as neighbours the defects are called F_n -centres ($n = 2, 3, 4, \dots$). The charge of F-centres are indicated by + or -.

Other defects are hole centre defects. The loss of an electron from an halogen ion leads to a lattice relaxation between two adjacent halogen atoms (X) neighbouring along the (110)-type direction. The defect can be described as a X_2^- molecule and it is called a V_K centre. The symmetry centre is two anion sites and it has a net positive charge compared to the perfect lattice. A X_2^- molecule may also occupy a single anion site, in which case it will interact strongly with its nearest neighbors along (110). This is a

so-called H centre and it may be regarded as a linear X_4^{3-} ion. This means that the hole is trapped along four halogen ions along the (110) direction.

2.8 Calculation of lifetime

Lifetime is a very important property of the excited state. For allowed emission transitions it is short, for forbidden transition it is long. For a two-level system the population of the excited state decreases according to [19]

$$\frac{dN_e}{dt} = -N_e P_{eg} \quad (2-3)$$

Where N_e is the number of luminescent ions in the excited state after an excitation pulse, t is the time, and P_{eg} is the probability for spontaneous emission from the excited state to the ground state.

Integration yields,

$$N_e(t) = N_e(0) e^{-P_{eg}t} \quad (2-4)$$

Equation (2-3-2) is also written as

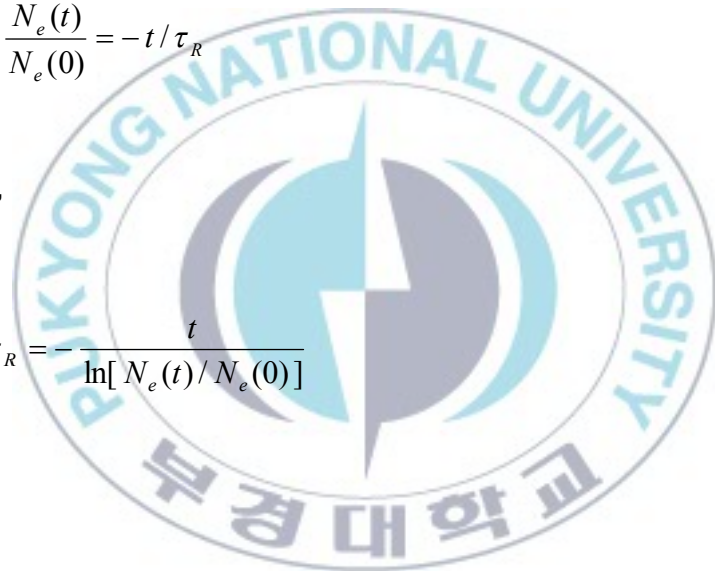
$$N_e(t) = N_e(0)e^{-t/\tau_R} \quad (2-5)$$

Where τ_R is the radiative decay time. Natural logarithm of the equation (2-3-3) is

$$\ln \frac{N_e(t)}{N_e(0)} = -t/\tau_R \quad (2-6)$$

Thus,

$$\tau_R = -\frac{t}{\ln[N_e(t)/N_e(0)]} \quad (2-7)$$



3. Experimental

3.1 Crystal growth by Czochralski method

The Czochralski method is named after Polish scientist Jan Czochralski, who discovered this method in 1916 while investigating the crystallization rates of metal. It's a particular method of crystal growth, wherein a seed is touched on top of the melt contained in a crucible and drawn slowly at a controlled rate. Then the crystal grows below the seed. The seed and the crystal are often rotated to provide a uniform growth environment. The rate of rotation and pulling speed can be changed to get single crystals with different diameters. Fluid motion within the melt is important because it affects the quality of the crystal. The flow driving forces considered are buoyancy, crystal rotation and surface-tension gradient.

The compound LiBaF_3 was firstly made by solid reaction method, and the compound melts incongruently and a single crystal must be grown from a non-stoichiometric melt to avoid other phase precipitations. Neuhaus et al [27] and Leckebusch et al [28] proposed that crystal growth can be achieved by a programmed non-linear temperature decrease of the melt considering the liquid's line (C-E) from the phase diagram of LiF-BaF_2 system (figure.3.1). In this work the preparation of Mn-doped LiBaF_3 with good

optical quality are presented. We use a non-linear program with 3 different temperature rates.

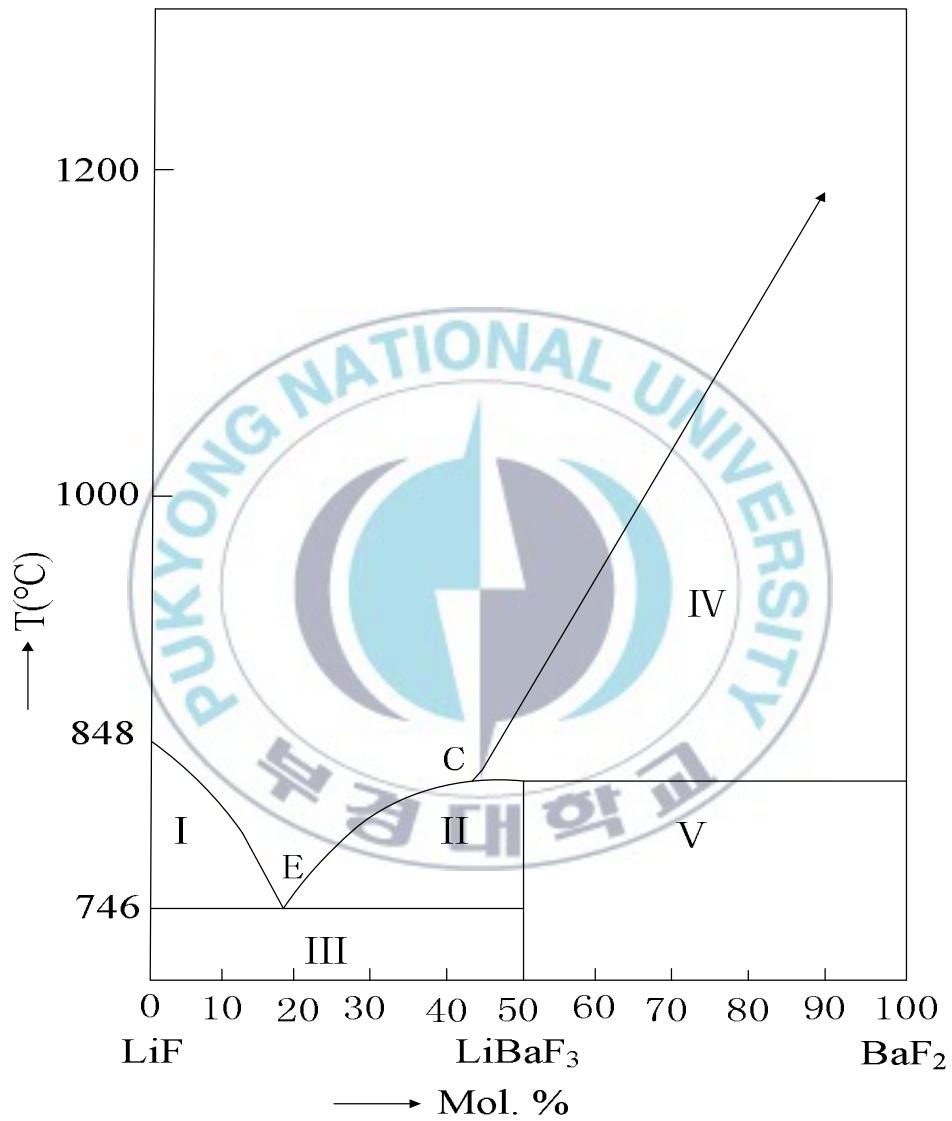


Fig. 3.1 Phase diagram of the LiF-BaF₂ system [6]. I .LiF(S) +LiBaF₃(L). II .LiBaF₃(S+L). III.LiF(S)+LiBaF₃(S). IV.BaF₂(S)+LiBaF₃(L). V.LiBaF₃(S)+BaF₂(S). CE is the Two-phase Curve (Melting Curve).

A study of figure.3.1 shows that LiBaF_3 melts incongruently and any single crystal must be grown from a melt containing an excess of LiF to avoid the precipitation of BaF_2 . This excess of LiF must be maintained throughout the growth period.

3.2 Growth procedure of the LiBaF_3 single crystal

The pure and Mn-doped LiBaF_3 powders were prepared by solid state reaction method at high temperature. Determination of the melting point and the rate of raising temperature were carried out by DTA (PERKIN-ELMER, DTA 7e). Lattice parameters and phase identification were measured by XRD (PHILIPS, X'Pert-MPD System). The crystals were grown in the platinum crucible which was laid in the chamber filled with high purity Argon gas. The all grown crystals were cut to standard samples (3×3×2 mm).

3.2.1 Synthesis of LiBaF_3 precursor powder

According to the study of above mechanism of LiBaF_3 crystal growth, we made the precursor powder with the mixture of non-stoichiometric ratio (40% BaF_2 and 60% LiF). Two kind of different concentrations of the MnF_2 doped in LiBaF_3 were 0.05mol% and 0.5mol%. The admixture was placed in a reagent bottle. Then, the reagent bottle was laid on a ball miller in order to

mix the powder completely. After the mixing, we firstly got the DTA data, as shown in figure 3.2 to analysis the melting point of the precursor. From the figure.3.2, it easy to get the melting point(784 °C) of mixed powder which it is very important parameter for the next of crystal growth.

The mixed powder was pre-heated at 500 °C with the holding time 10 hours for three times in the vacuum atmosphere to eliminate water trace contamination, and after each sinter, we grinded the compound to let the reactant mix well and reaction reacted completely. After several of sinter at 500 °C , we got the precursor for the next step of growth.

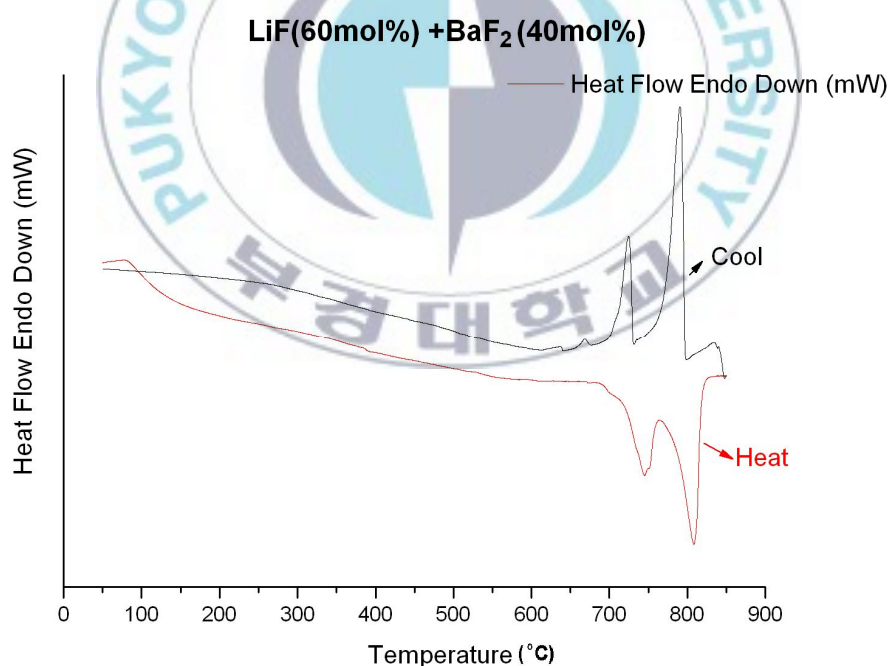


Fig. 3.2. Differential thermo-gravimetric analysis (DTA) of $\text{LiF}-\text{BaF}_2$ system. In the heating curve, there are two absorption peaks, and the stronger one is the melting-point-peak.

3.2.2 Crystal growth of LiBaF₃ single crystals

The Czochralski method began with Mn-doped LiBaF₃ powder which was prepared by solid state reaction method. The apparatus of the Czochralski method is shown in the figure 3.3. The precursor powder was placed in platinum which was put in a steel chamber and encased with some aluminum balls. Next, the chamber was closed and the pump was turned on to get a vacuum atmosphere. When the powder was heated to 300 °C, the chamber was filled with argon gas (1~1.5 kgf/cm²) and the gas was pumped out for 3 times to get a pure argon gas atmosphere. The powder was heated up to a set temperature which is 10 or 20 °C lower than melting point, then we increased the temperature to the melting point slowly (1~2 °C/min) by changing heating program control to manual control [29].

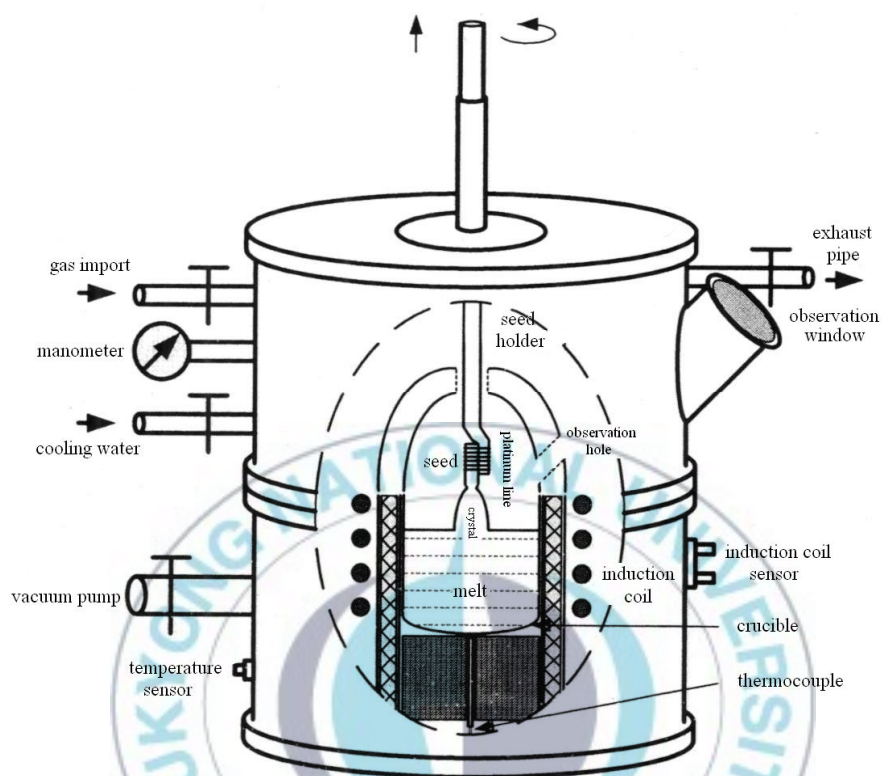


Fig. 3.3 Illustration of crystal growth chamber. Pure LiBaF_3 crystal seeds were used to grow single crystals.

When the powder was melted, a small seed crystal mounted on the end of a rotating shaft was slowly lowered until it just dipped the surface of the red-hot melt. Then, the rotating rod was drawn upwards with a speed (1 mm/h). During the process of growing, we can adjust temperature, rotation speed and pulling speed to change shape of crystal. In the first 8 hours (stage 1), we set a pulling speed of 0.6 mm/h, and in the next 25 hours (stage 2), pulling speed was changed to 0.4 mm/h, finally changed the

pulling speed from 0.4 mm/h to 3 mm/h or more high in 10 hours (stage 3) to make the crystal separated from the melting liquid. Also in the temperature decreasing speed is different: in the stage 1, the speed is 0.5 °C/h, while in stage 2 is hold the temperature for 25 hours, and the final stage 3, the increasing speed of temperature is 2 °C/h.

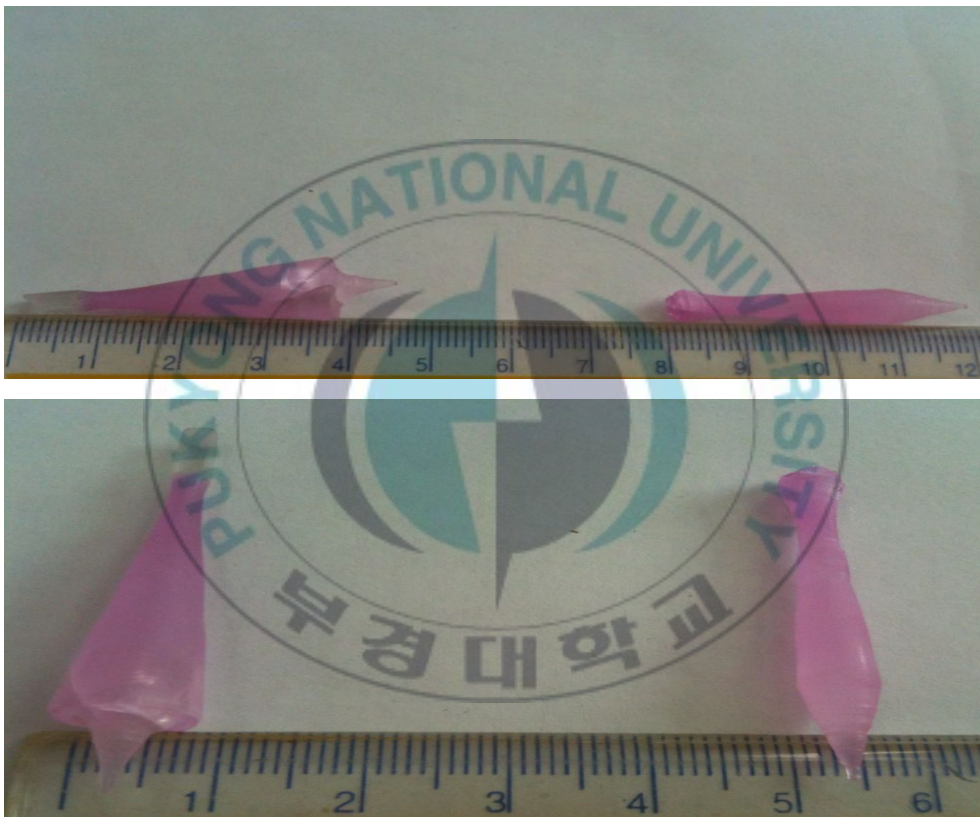


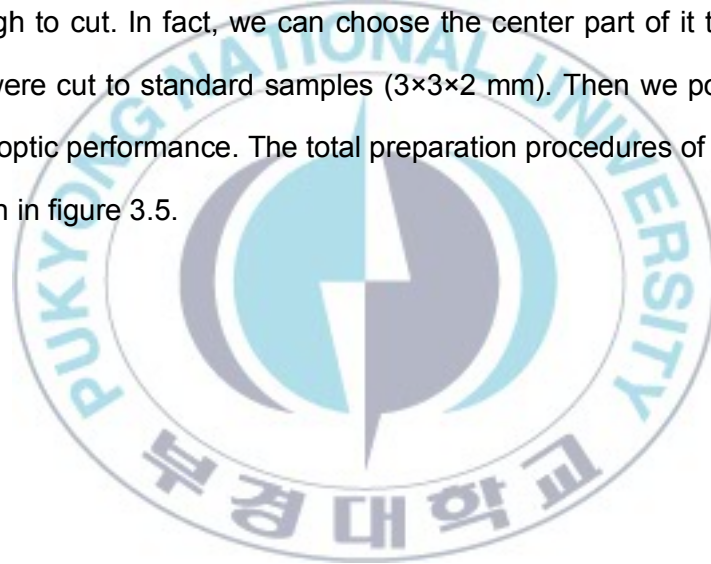
Fig. 3.4 LiBaF₃ single crystal. Though there are some cracks at the bottom of this crystal and the size is enough to cut.

After the crystal separated from the melting liquid, keep the crystal at a position which is 0.5~1 cm higher than the melt for 2 h to get symmetrical temperature gradient. Finally, the crystal was slowly cooled to room

temperature at the speed of 1 °C/min. Two crystals grown by the Czochralski method is shown in figure 3.4.

3.2.3 Sample machining

We grew LiBaF_3 single crystals with four different concentrate (0.05, 0.5mol%). Although there are some small cracks inside the crystal, their size are enough to cut. In fact, we can choose the center part of it to test. The crystals were cut to standard samples (3×3×2 mm). Then we polished it to get good optic performance. The total preparation procedures of the sample are shown in figure 3.5.



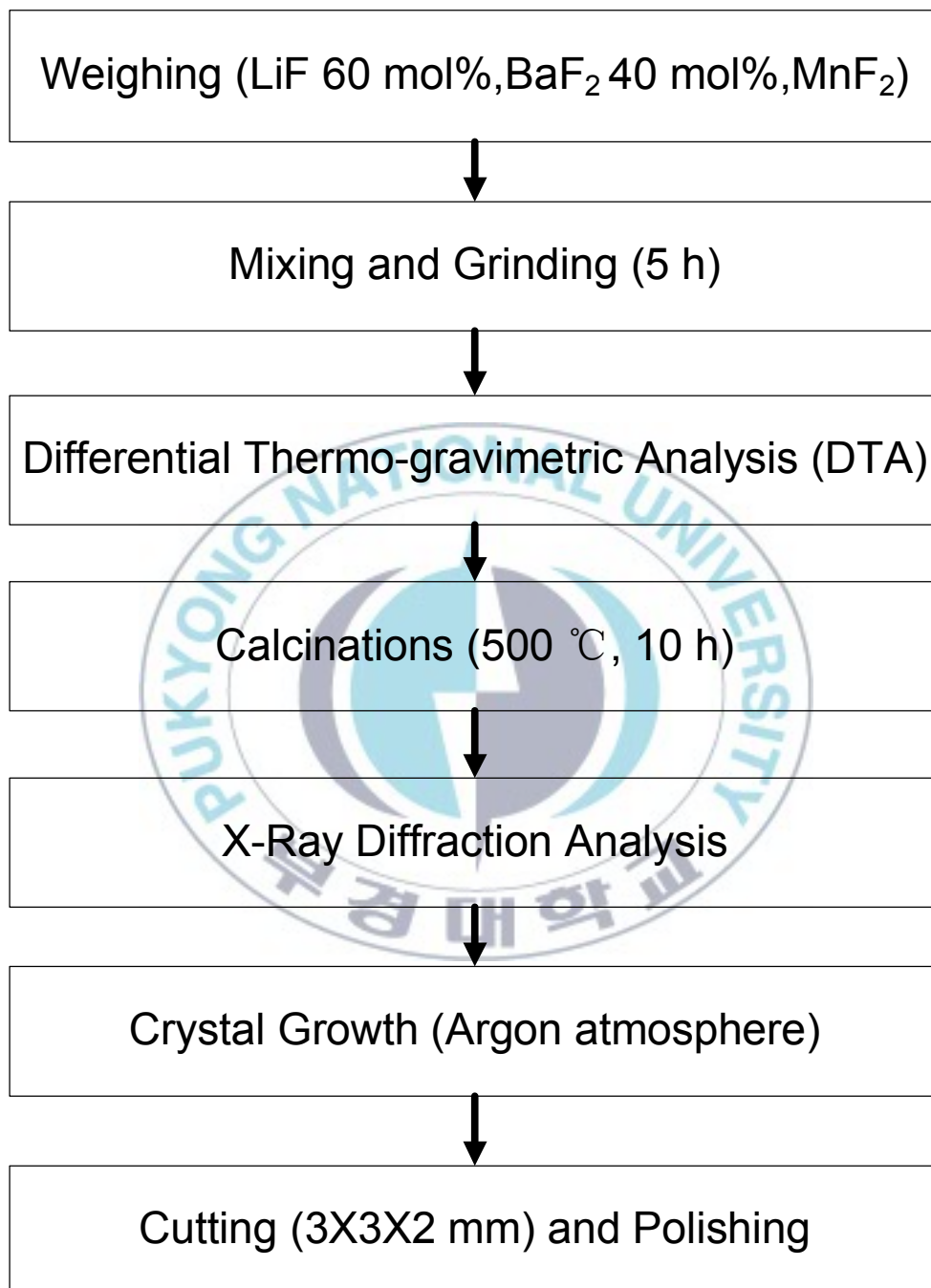


Fig. 3.5 Preparative procedures diagram of the LiBaF₃ single crystal.

3.2.4 Several factors influencing the crystal growth

3.2.4.1 The initial temperature cooling rate

As mention above, we separate the growth process into three parts. In the first stage within the 8 hours, we set the temperature cooling rate as 0.5 °C/h. In the stage, the temperature cooling speed depends the size and cracks condition in neck part of crystal. If the speed is high, the neck would be short and small, which made against the next growth stage of body part of crystal. And small neck would be easy to increasing probability of crack appearance which affects the crystalline homogeneity and optical transmission. However, if the speed is slow, the neck would be so big that the growth breaks off because the heavy weight of crystal.

According to the reasons above, we set the proper temperature cooling speed rate in the stage two and stage three are 0°C/h and 2°C/h respectively.

3.2.4.2 Rotation and pulling speed

Different rotation speeds result in different interface shapes of the growing crystal. For the LiBaF₃ single crystal used of the Czochralski method, the solid interface becomes concave towards the melt for high

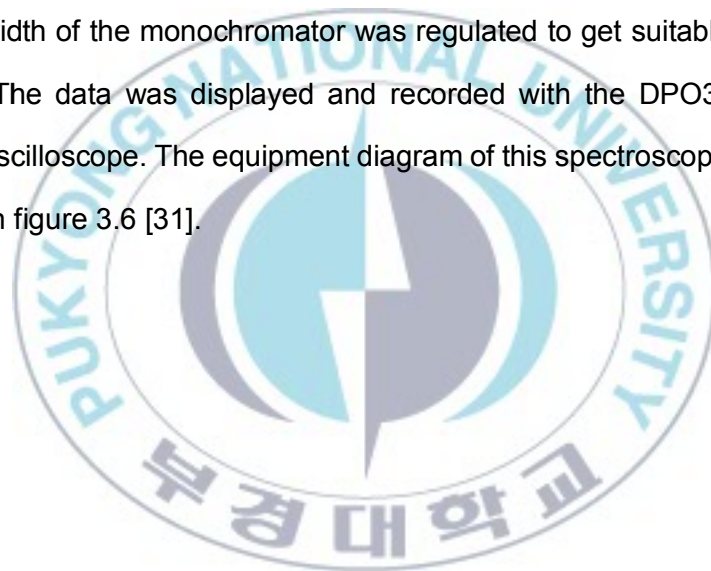
rotation rate, flat for middle rate and convex for low rotation rate [30]. We can get a bigger crystal by changing the rotation speed. For different points at the face of the melt, the temperatures are different. Using faster speed might cause asymmetry of the temperature which results in more defects inside the growing crystal. But the crystal is very difficult to grow at low rotation speed. After repeating many times, we found 30-40 rpm is a best choose.

Pulling speed is also a very important factor for crystal growth by the Czochralski method. The difference of the temperature from bottom to top of the crucible is very big without platinum thermometer. Thus, the pulling speed we used is lower than 1 mm/h. Otherwise, the optic properties of the crystal is not good. So the pulling speed in the stage one, stage two and stage three are 0.6 mm/h, 0.4 mm/h and from 0.4-3 mm/h respectively.

3.3 Fluorescence dynamics spectrometer

The spectroscopic measurements of $\text{LiBaF}_3:\text{Mn}^{2+}$ single crystals were performed by the pulsed Nd: YAG laser at 266 nm and 355 nm and 532 nm (Spectron Laser System SL802G), together with the Dye laser (Spectron Laser Systems, Model SL4000B/G). The samples were attached to a holder which was placed in a helium gas flow cryostat in a variable temperature

region (10-300 K). The pulsed Nd: YAG laser beam with 25 mJ pulse energy was focused and crossed the polished faces. The emission spectra were measured by monitoring the emission intensity in different wavelengths under the pulsed laser excitation. The lifetimes were also measured to give the additional explain for the different energy levels of $\text{LiBaF}_3:\text{Mn}^{2+}$ samples. The luminescence was dispersed by the 75 cm monochromator (Acton Research Corp. Pro-750) and multiplied by the PMT (Hamamatsu R928). The slit width of the monochromator was regulated to get suitable emission spectra. The data was displayed and recorded with the DPO3054 digital storage oscilloscope. The equipment diagram of this spectroscopy system is showed in figure 3.6 [31].



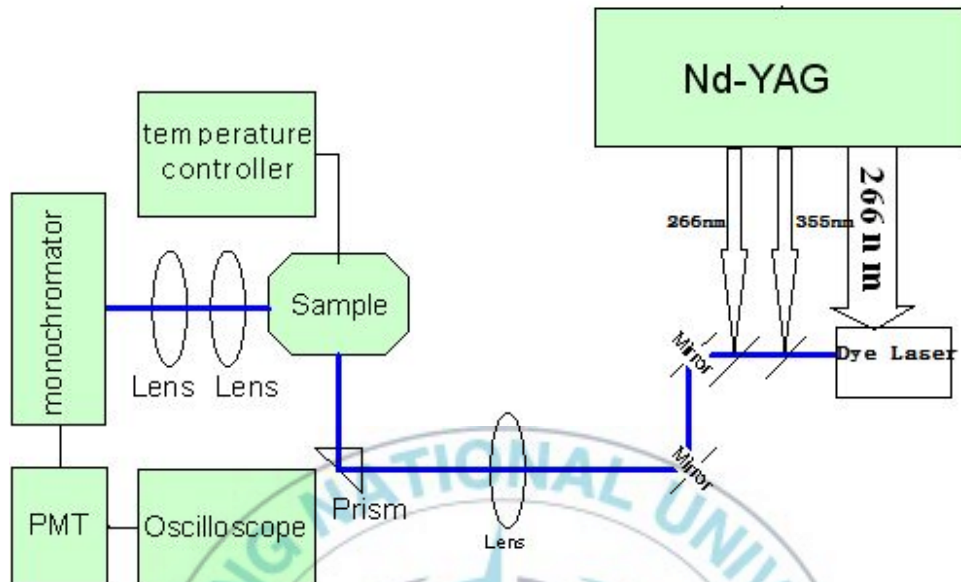


Fig. 3.6 The equipment diagram of spectroscopy measurement system. The laser with 25 mJ energy was focused by a lens and crossed two polished faces of the $\text{LiBaF}_3:\text{Mn}^{2+}$ single crystal which was cooled by a helium gas flow cryostat.

3.4 Crystal structure characterization

X-ray diffraction (XRD) is one of the most important characterization tools to determine crystal structure and lattice parameters of any crystalline compound [32].

Each crystalline solid can be presented as an infinite regular three-dimensional distribution of atoms in space. They form a series of parallel planes separated from one another by a distance d , which exists in a

number of different orientations [33]. In XRD, as a beam, which is based on constructive interference of monochromatic X-rays and a crystalline sample, travels through any substance, the resulting diffracted beams are detected and the intensity decreases with the distance traveled through the substance. If the sample is crystalline, the interaction of the incident rays will produce constructive interference (and a diffracted ray). Meanwhile, detected intensities of diffracted beams will vary in different directions. According to Bragg's Law ($n\lambda = 2d \sin\theta$), which relates the wavelength of electromagnetic radiation (λ) to the diffraction angle(θ) and the lattice spacing in a crystalline sample (d), a unique diffraction pattern is produced, characteristic of the crystal structure of the sample .

In this thesis, the XRD profile were measured within the range of 10-70° in step of 0.02° using X-ray diffractometer (X'PERT PRO, PHILIPS) with $\text{CuK}\alpha = 1.5406 \text{ \AA}$ radiation at 40kV and 30 mA. The data obtained from the XRD were compared with the Joint Committee Powder Diffraction Standards(JCPDS) cards and the unit cell parameters were calculated using Powder-X diffraction analysis software: Jade 5.

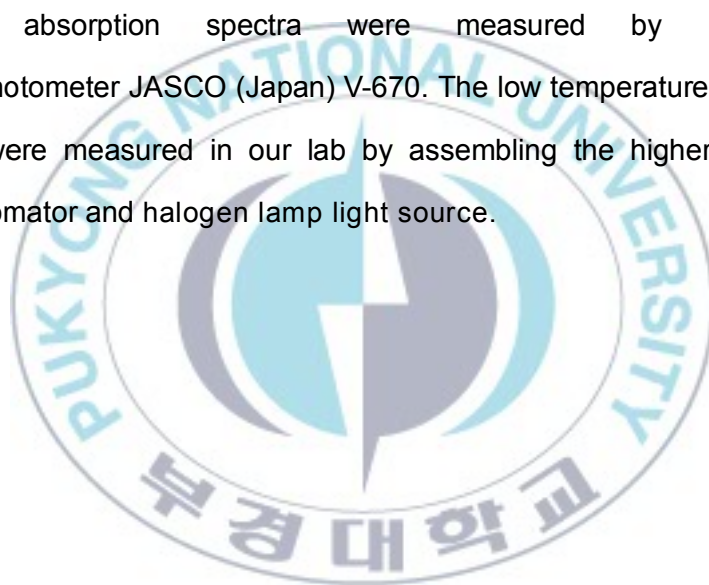
3.5 Luminescence spectrometer

The room temperature photoluminescence excitation (PLE) and photoluminescence (PL) spectra of the samples were recorded on a

luminescence spectrometer (Perkin Elmer (U.S.A.), LS50B) and a PTI (Photon technology international (U.S.A.)) fluorimeter using a Xe-arc lamp with a power of 60 W.

3.6 Absorption spectrometer

The absorption spectra were measured by UV-Vis/NIR Spectrophotometer JASCO (Japan) V-670. The low temperature absorption spectra were measured in our lab by assembling the higher resolution monochromator and halogen lamp light source.



4. Results and discussion

4.1 X-ray diffraction analyse

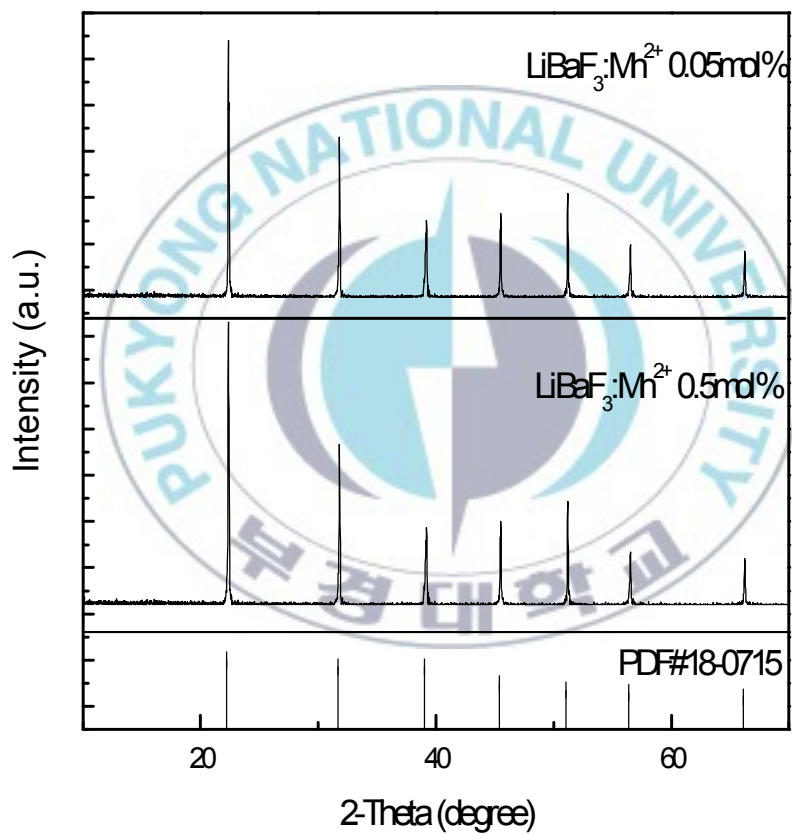


Fig. 4.1 XRD patterns of $\text{LiBaF}_3:\text{Mn}^{2+}$ 0.05mol% and 0.5mol%

The crystal structure of LiBaF_3 has been refined to be cubic, space group

Pm-3m(221) with $a = b = c = 3.995 \text{ \AA}$, $V = 63.8 \text{ \AA}^3$ The XRD patterns of LiBaF_3 with Mn^{2+} doping concentration of 0.05, and 0.5mol% are shown in Fig. 4.1. In this work, we think that the Mn^{2+} ions occupy the Li^+ ion sites ($r=0.76 \text{ \AA}$) with remote charge compensation because of different changes or Ba^{2+} sites ($r=1.61 \text{ \AA}$) as Mn^{2+} radius ranges from 0.66 \AA to 1.1 \AA . depending on its coordination. All the reflections are indexed on the basis of an cubic unit cell of LiBaF_3 (JCPDS Card: 18-0715). No crystalline impurity phase could be detected in any sample, indicating that the grown crystals are single phase and the doped Mn^{2+} ions have no influence on the crystal structure of LiBaF_3 .

Using the XRD analyze software Jade 5.0, we calculate the cell parameter as a application of scherrer equation $D_{hkl} = K \lambda / \beta \cos\theta$, where D_{hkl} is the length along the surface direction of (hkl), K is the shape factor, typically 0.89, λ is the X-ray wavelength, 1.5406 \AA , β is the line broadening at half the maximum intensity (FWHM) in radians, and θ is the Bragg angle. So we got that the material is cubic structure with $a=b=c=3.98405 \text{ \AA}$, volume is 63.18 \AA^3 . This result mach very well with the JCPDS card: 18-0715.

4.2 Fluorescence Testing results

4.2.1 Absorption spectra

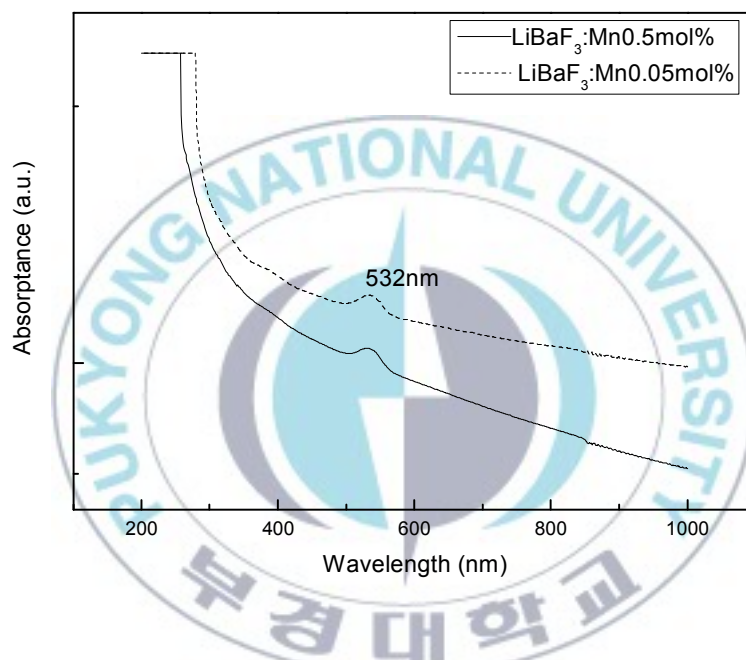


Fig. 4.2 Absorption spectra of LiBaF₃:Mn0.05 mol% and Mn0.5 mol% at Room temperature.

The absorption spectra was measured by UV-Vis/NIR spectrophotometer (JASCO (Japan), V670) shown in the figure 4.2 at room temperature. From the absorption spectra, there is a broad band peak centered at 532 nm. Although the concentration of Manganese is different, the peak position is almost the same which could ascribe as the defects

absorption in the crystal, which could be the reason why the crystal color is pink.

In figure 4.3, the excitation spectra under different temperatures were compared. The absorption spectra were measured by the tungsten lamp in the range of 400 to 800 nm.

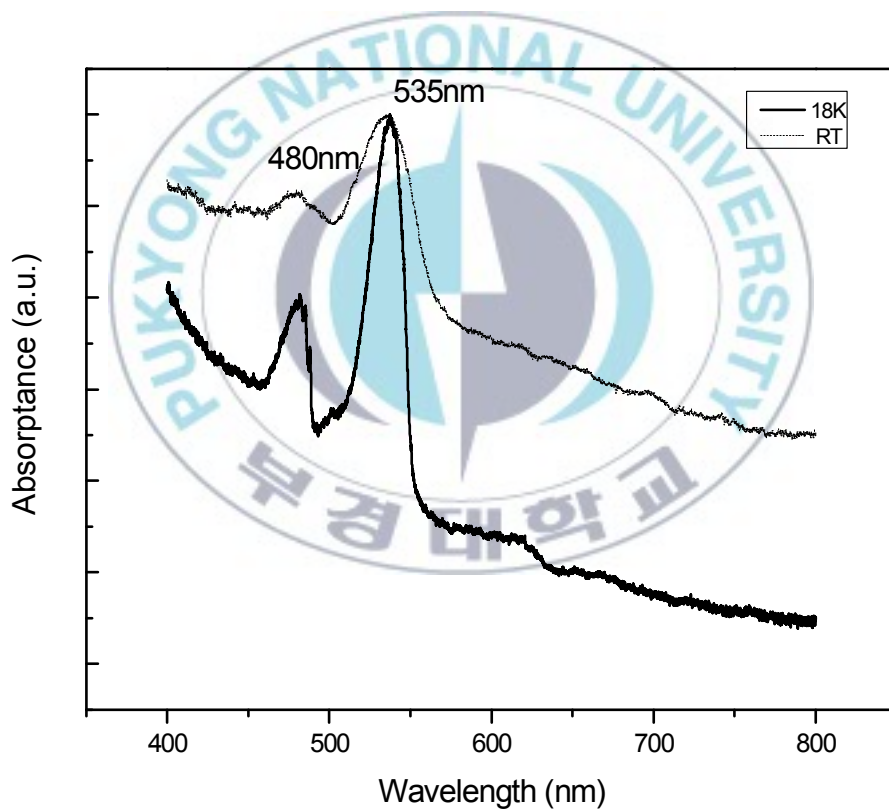


Fig. 4.3 Excitation spectra of LiBaF₃:Mn_{0.05}mol% at RT and 18K

From the figure 4.2 and figure 4.3, the absorption peak centered at around 532nm was detected at room temperature. No obvious different in absorption spectra was found at room temperature, although the manganese doping concentration was different. This peak is associated with the defect absorption in the crystal mentioned above. At the low temperature 18 K, one more peak was found at around 480 nm, which could be ascribed as ground state ${}^6A_{1g}(S)$ ground to excited state ${}^4T_{1g}(G)$. It is also possible that this band around 480 nm is because of the defects absorption in the crystal. This could be proved that in the emission spectra under the excitation of Argon 476.5 nm (see details in figure 4.7). Compared the difference of absorption spectra under different temperatures, some peaks were quenched because the increasing temperature, which could be described as temperature quenching. At relative high temperature, the vibration is increasing as a result of temperature quenching. The energy absorbed consumed in the form of vibration.

4.2.2 Mn-related Complex

$3d^n$ transition metal ions utilized in efficient luminescent material are preferably $3d^5$ (Mn^{2+} , Fe^{3+}) or $3d^3$ (Mn^{4+} , Cr^{3+}) elements. Both have the lowest excited state, which is responsible for emission, in the visible spectral region. Mn^{2+} ions exhibit wide-range emission from 500 to 800 nm, depending on the host crystal. Hundreds of luminescent materials, in

particular those used in fluorescent lamps have been developed based on Mn^{2+} as dopant or co-dopant with efficient energy transfer capabilities [37-39].

In this section divalent Manganese is evaluated as optically active ion in $LiBaF_3$ crystals. As talk above, the emission from the excited state to ground state is spin forbidden ($\Delta s=1$). The crystalline field perturbs the pure states and looses the selection rules [39]. Anther saying is that the selection rules are relaxed through an exchange mechanism (spin-spin interaction) and a vibronic mechanism (coupling with odd lattice vibrations which partially destroy the inversion centre) [40]. In comparison with 4f elements, the 3d transition metals show a much stronger electron-phonon coupling. Hence the rich energy level structure of Mn^{2+} allows nonradiative relaxation even at liquid helium temperature to the lowest excited state ${}^4T_{1g}$ (G) and subsequent emission ${}^4T_{1g} \rightarrow {}^6A_{1g}$ to the ground state. Several emission bands at different energies are observed, if Mn^{2+} is incorporated into different crystallographic sites. The emission bands have typically a broad FWHM without any features, and are of a non-Gaussian Pekar shape [40]. This is due to the strong electron-phonon coupling of the 3d ions which prevents the observation of sharp electronic or vibrational lines, as opposed to rare earth ions.

Crystals may have more than one lattice site, which is occupied by the

dopant ions. If both sites are strongly varying in symmetry or size, the spectrum may change significantly. This is especially true for the 3d ions which are sensitive to the crystal field. Some crystals have intrinsically sites of the same point symmetry, which lead to slightly different emission energies. Such sites can be introduced by charge compensation as well, if the substitutional site has a different ionization state.

In our grown crystal, LiBaF_3 has two sites, one is Li^+ site, and another is Ba^{2+} site. In pure LiBaF_3 both sites have O_h point group symmetry [43]. As we mentioned above, the Mn^{2+} has high probability to substitute the Li^+ site, giving birth to the charge compensation defects. If Mn^{2+} substitutes the Li^+ site, that is to say the crystal field for the Mn^{2+} is relative high crystal field, which gives birth to the red emission. A fraction of Mn^{2+} could be substituted into the Ba^{2+} . Ba^{2+} site in the LiBaF_3 crystal has O_h point group symmetry; however, if the Mn^{2+} ion in this surrounding is situated on a considerably larger lattice site, a lower crystal field is expected, resulting in a shift of the emission towards higher energy [42]. Radius of Ba^{2+} is 1.61\AA while the radius of Mn^{2+} is 0.8\AA . Another reason should be contribute for proving the emission shift to high energy is that lowering of symmetry at Mn^{2+} site, because of the charge-compensating defects [49]. Also the Mn^{2+} luminescence in the cubic lattice showing a green emission is investigated by DIETRICH LANGER [41]. In our work, two broad bands were detected which are ascribed to Mn^{2+} emission. One band centered at 510 nm , while

another one is located at 750 nm.

4.2.2.1 Band A — green emission

(a) Emission

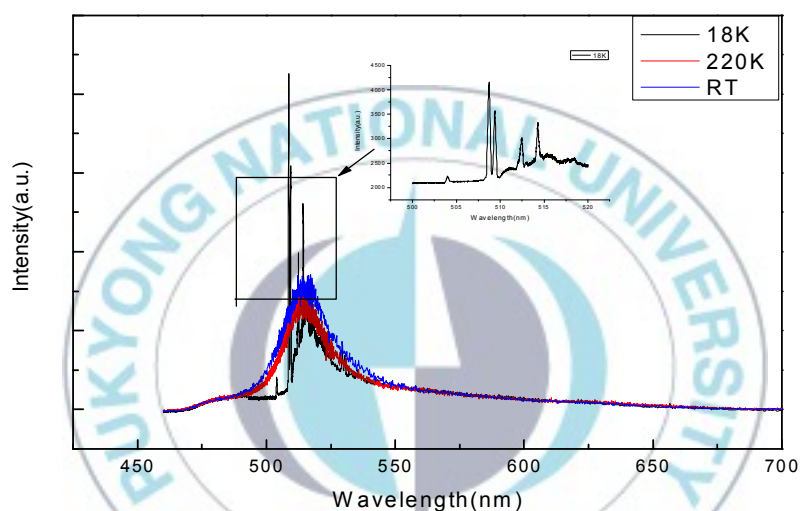
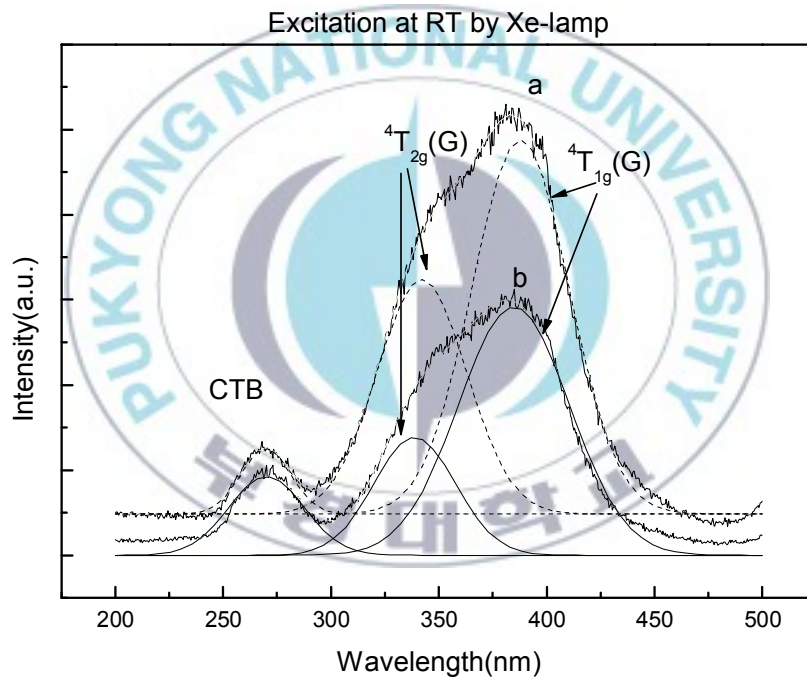


Fig. 4.4 Emission spectra of LiBaF₃:Mn excited by 355 nm laser at different temperature.

Here in the figure 4.4, the Mn²⁺ activator center has the green emission centered at 515 nm, although the doping concentration is different, no obvious difference was observed. With increasing temperature from 18K to RT, the band shifts slightly to shorter wavelength of ~3 nm. The blue shift with increasing temperature is ascribed to the thermal population of Mn²⁺ ions at the sites with higher excited states, which are often observed in

Mn²⁺- or Eu²⁺-doped host lattice with inequivalent crystallographic sites. What is more, the FWHM is decreasing with the increasing of temperature. Mn²⁺ in the cubic lattice substitute the Ba²⁺ site and the broad band located at 515 nm appears.

(b) Excitation



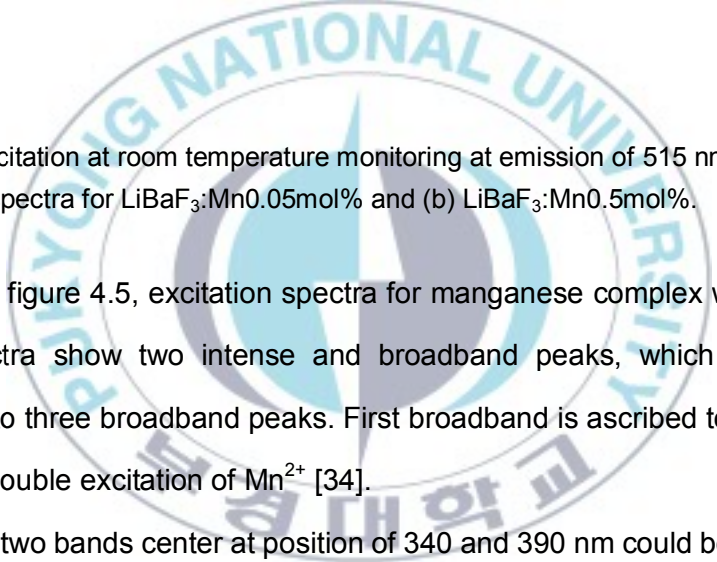


Fig. 4.5 Excitation at room temperature monitoring at emission of 515 nm. (a) is the excitation spectra for LiBaF₃:Mn0.05mol% and (b) LiBaF₃:Mn0.5mol%.

In the figure 4.5, excitation spectra for manganese complex was given. This spectra show two intense and broadband peaks, which could be divided into three broadband peaks. First broadband is ascribed to CT band [35] or a double excitation of Mn²⁺ [34].

The other two bands center at position of 340 and 390 nm could be ascribed to the excited state of ⁴T_{2g} (G) and ⁴T_{1g} (G), respectively.

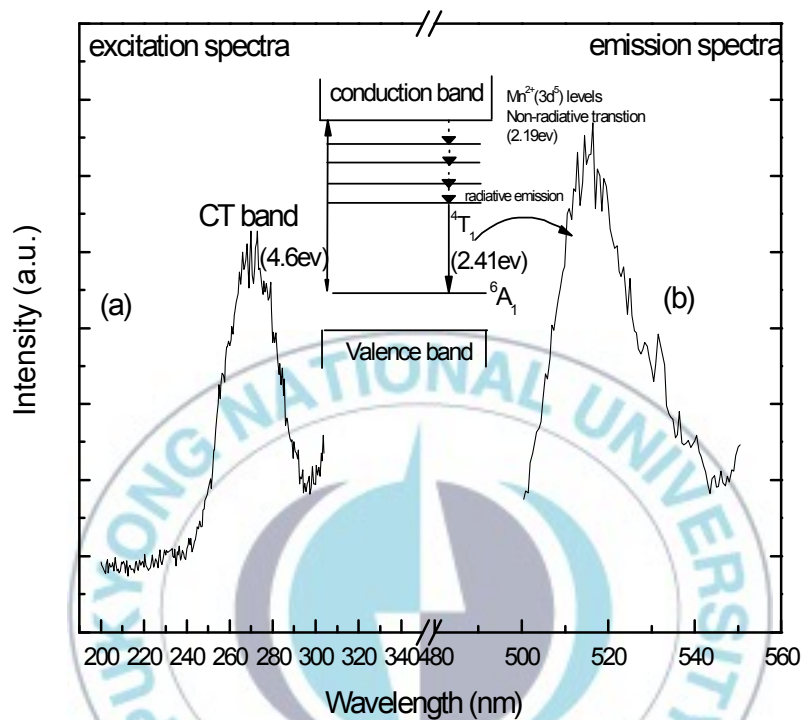
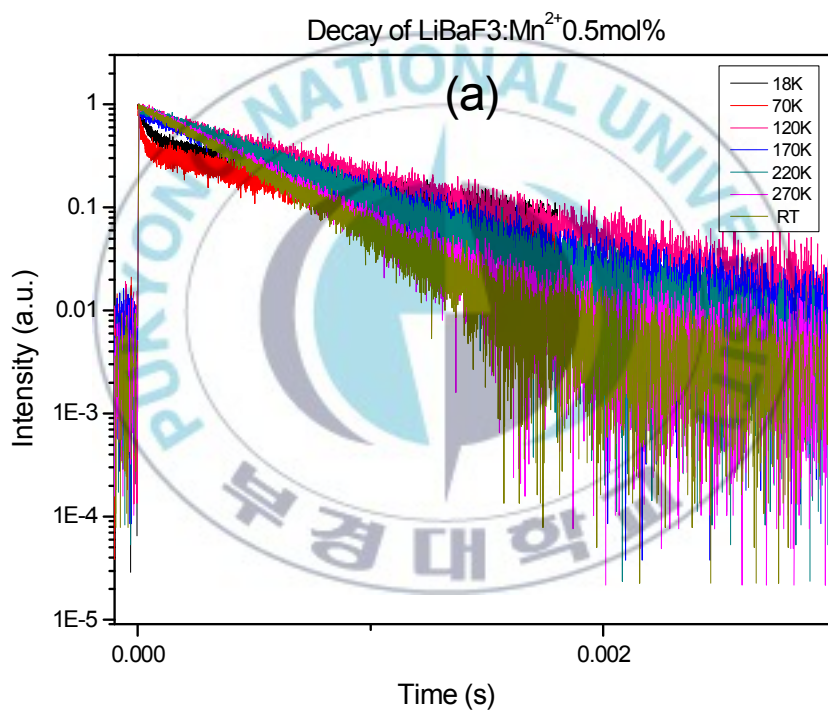


Fig. 4.6 PL (a) excitation and (b) emission spectra of LiBaF₃:Mn0.5mol%; (c) energy level scheme describing the excitation and emission spectra.

The electrons at the ${}^6A_1(6S)$ ground state of Mn^{2+} ions, which originate from the photo excited ionization of Mn^{2+} , are excited to the conduction band of LiBaF₃ by photons, and the free electrons in the conduction band relax back to the ${}^4T_1(4G)$ excited state through a non-radiative process [36]. Finally, this is followed by radiative transition from the ${}^4T_1(4G)$ excited state to the ${}^6A_1(6S)$ ground state, emitting green light (515 nm). The energy level

scheme of LiBaF₃: Mn in which the excitation through the CT band and the corresponding radiative and non-radiative transitions to realize green emission are shown in Figure 4.6 c.

(c) Lifetime



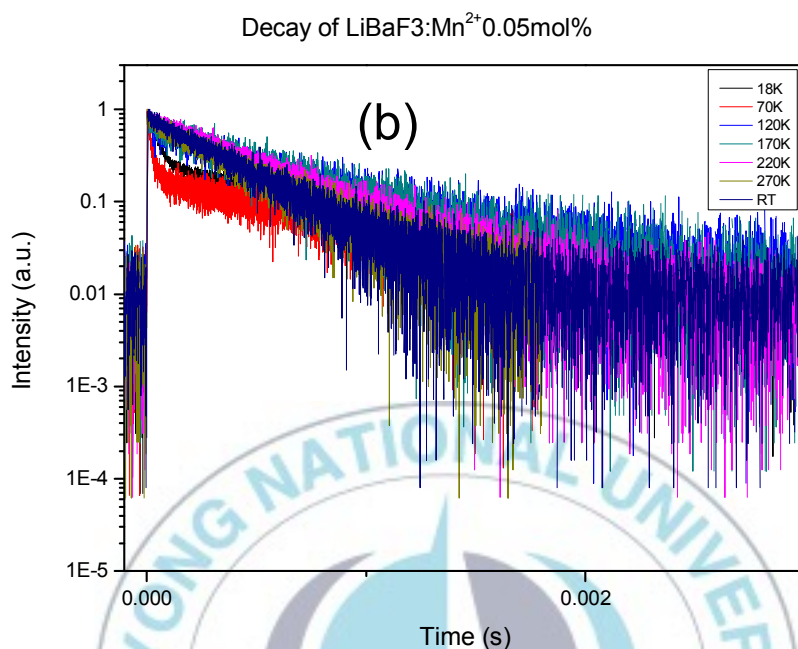
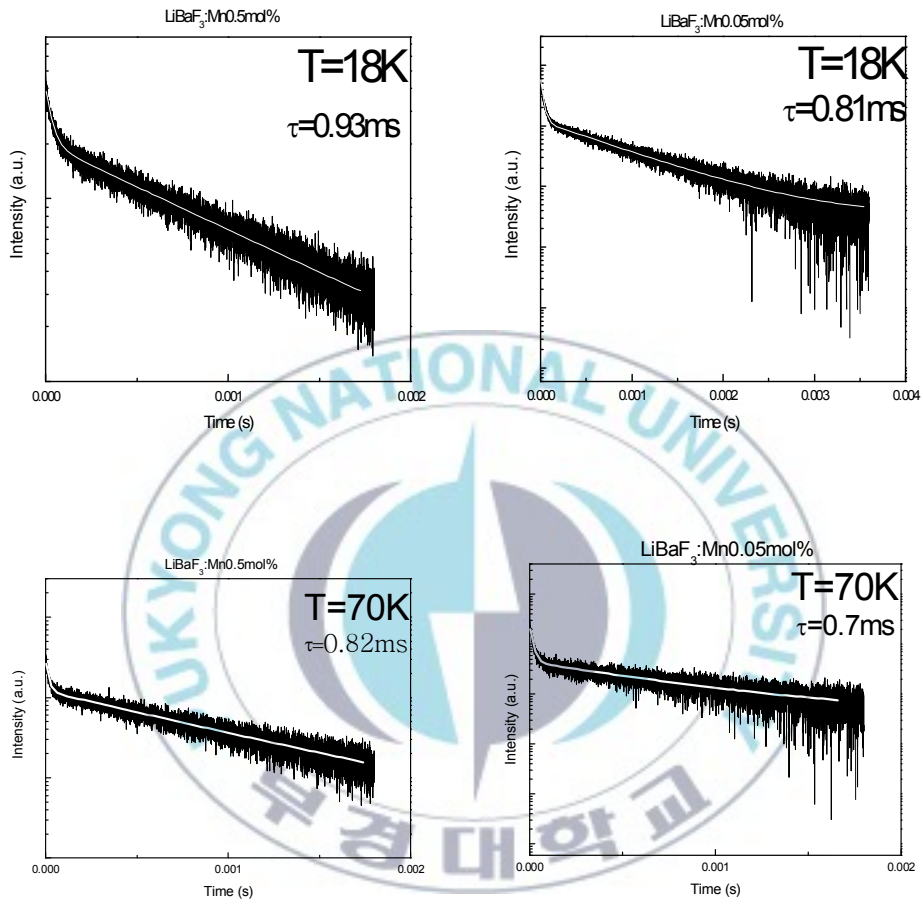
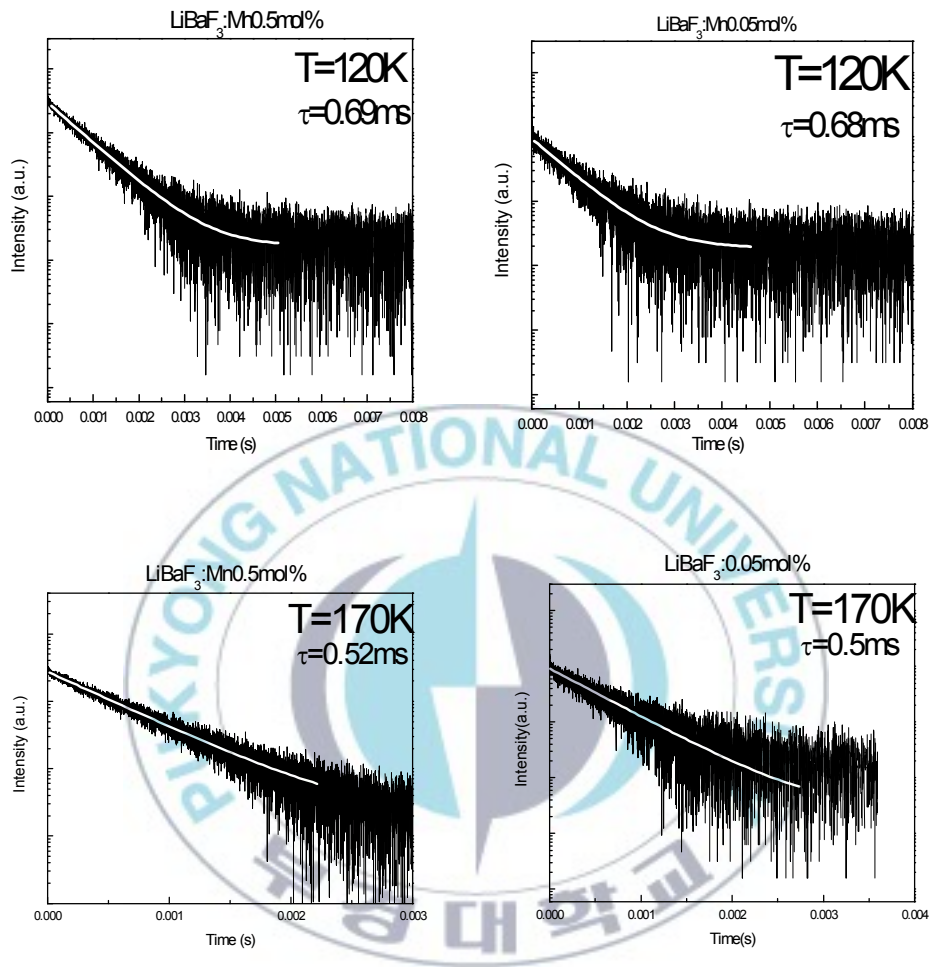


Fig. 4.7 Decay curves of Mn²⁺ luminescence at different temperatures; (a) LiBaF₃:Mn²⁺ 0.5mol%; (b) LiBaF₃:Mn²⁺ 0.05mol%

From the study of figure 4.7, the decay curves of Em510nm present a non-exponential curves from 18 K to 120 K, while the decay curves from 120 to 300K are single exponential. We fitted the exponential decay curve using equation 4 as mentioned above. Although the concentration of manganese doping in the crystal are different, the lifetime are almost the same, showing a typical temperature quenching behavior. The average decay time of nonexponential curve at the region of 120 to 300 K was evaluated using the equation (5) as mentioned above.

The fitting curves are shown in figure 4.8





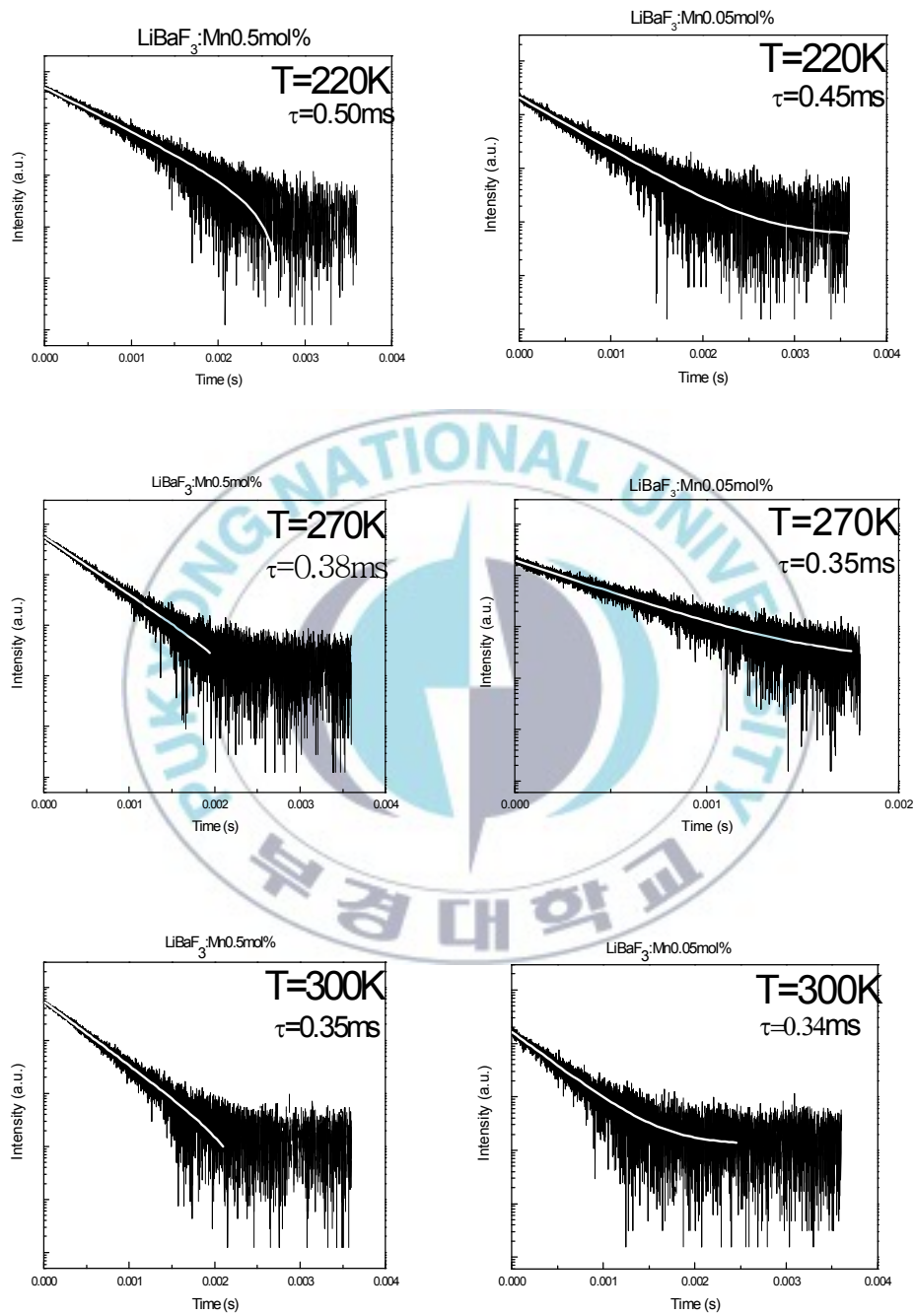


Fig. 4.8 Decay fitting curves of emission band 510nm at different temperatures

After the fitting of the decay curves, the lifetime of defects emission is 0.93 ms at 18 K and then drops with temperature increasing, presenting a typical temperature quenching behavior. See the details in the figure 4.9.

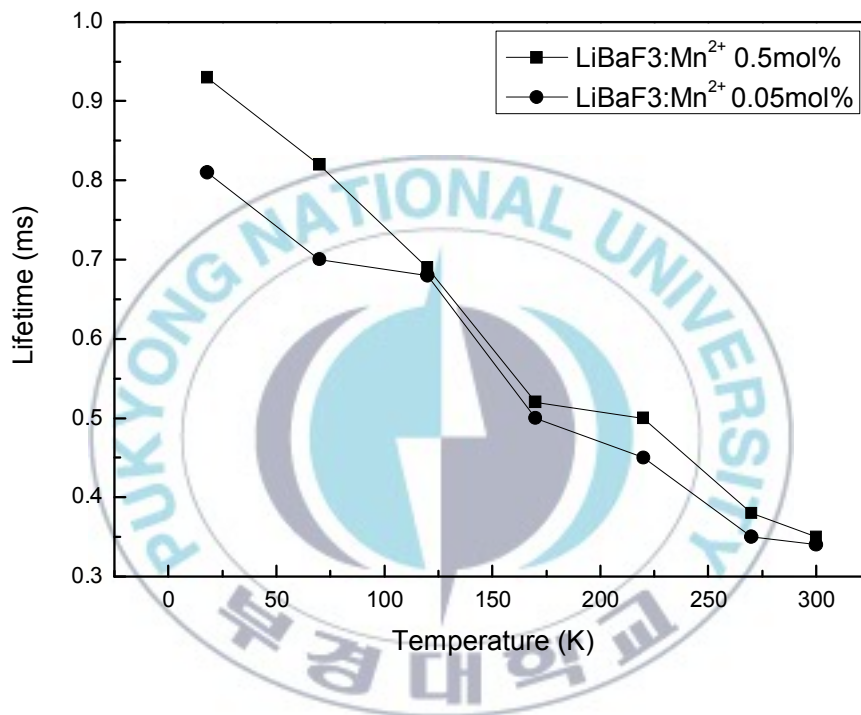
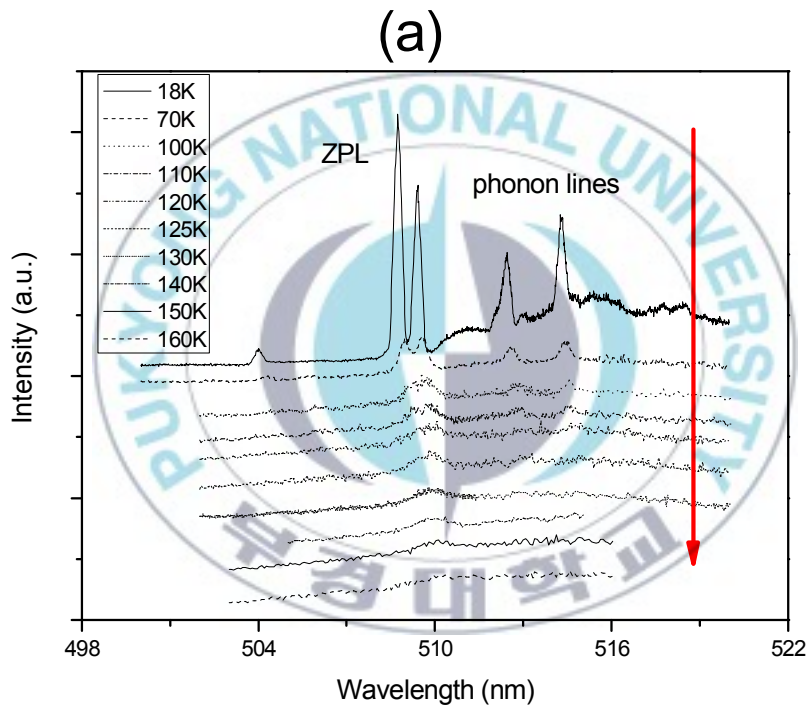


Fig. 4.9 The relationship between the lifetime and temperatures of 510nm emission band.

(d) Zero phonon line of the ${}^4T_{1g} \rightarrow {}^6A_{1g}$ transition

In various crystals zero-phonon transitions have been observed at low

temperature and rather low concentrations. Detailed vibronic fine structure was observed and first assigned to phonon-coupled electronic transitions in Mn^{2+} doped ZnS [47]. At low temperature a steep raise on the high-energy side is caused by the zero-phonon transition. Figure 4.4 show this sharp zero phonon lines were detected below 18 K.



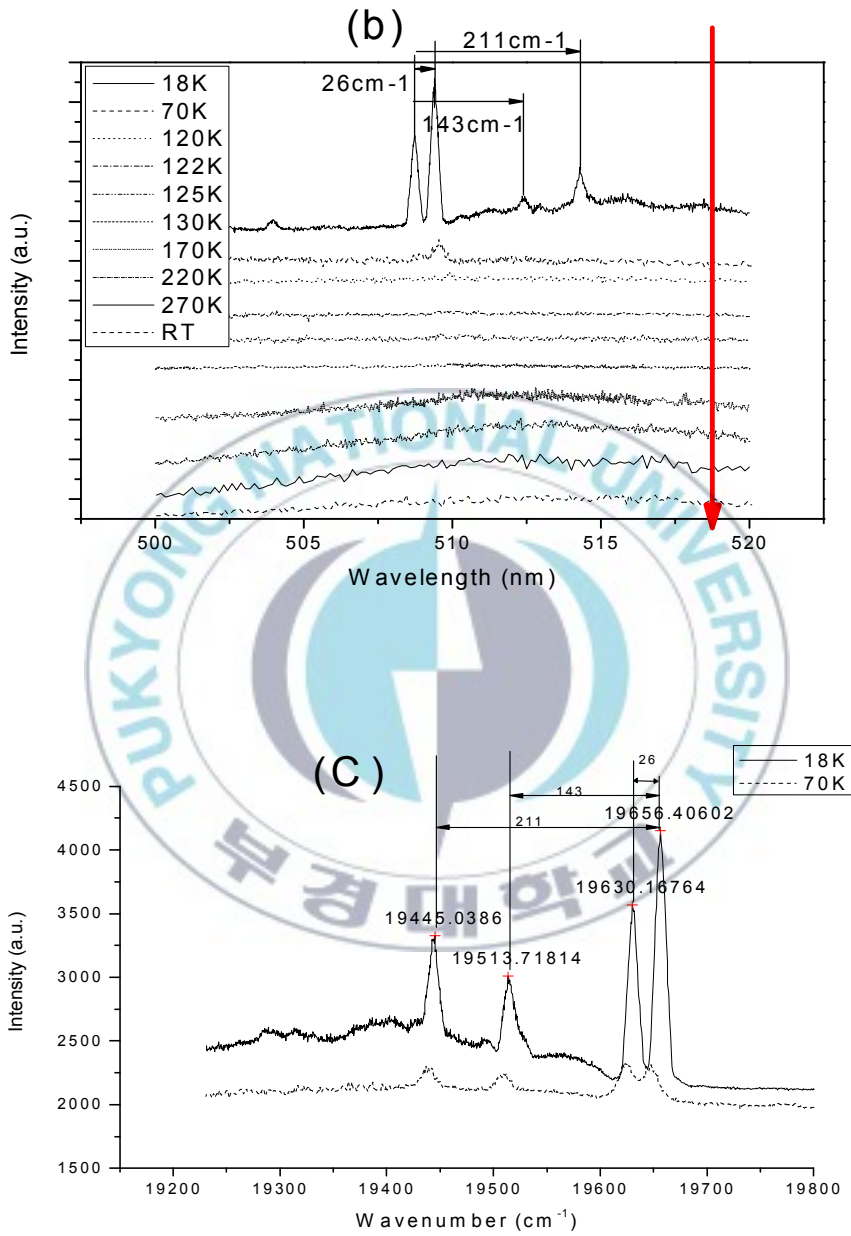


Fig. 4.10 Zero phonon line intensities under different temperature, (a) LiBaF₃:Mn0.5mol% (b) LiBaF₃:Mn0.5mol%, (c) energy difference in wavenumber.

As it shown in the figure 4.10, we recognized that the zero phonon line can be show at 70 K, and at the much lower temperature 18 K, the ZPL is separated. The line separation can be divided into three groups. There are 26 cm^{-1} , 143 cm^{-1} and 211 cm^{-1} respectively. All of these energy differences were assigned to TA, 2TA, LA and 3TA, LA+TA modes [47], respectively, which are summarized in table below.

Table 1 Phonon energies in LiBaF₃: Mn bands

transition	Line separation in cm^{-1}		
${}^4T_1 \rightarrow {}^6A_1$	26	143	211
modes	TA	2TA, LA	3TA, LA+TA

In the table, the low frequency suggests the assignment of a transverse acoustic (TA) mode. And higher frequencies of about 143cm^{-1} and 211cm^{-1} might actually be multiples of TA mode or a longitudinal acoustic (LA) mode or TA+LA modes, respectively.

4.2.2.2 Band B - Near IR emission

(a) Emission

Beside the Mn^{2+} having its green emission at 515 nm, it also shows its

characteristic luminescence at 750 nm. When the Mn^{2+} is substituted into the Li^+ site, the surrounding environment is octahedral crystal field. Figure 4.11 show the emission of Mn^{2+} when it in the O_h crystal field.

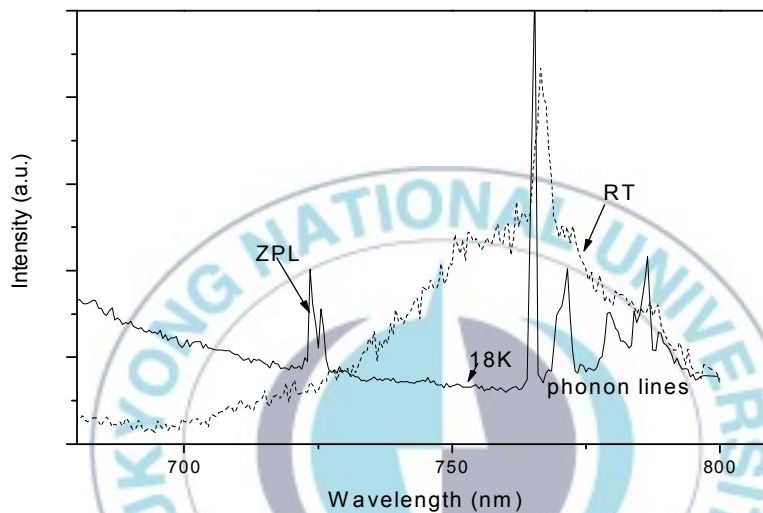


Fig. 4.11 Emission of $LiBaF_3:Mn$ at 300 K and 18 K excited by 532 nm pulse laser.

One special observation by comparing the emission spectra at room temperature and spectra at 18 K is that the intensity of broadband from 700 to 800 nm is decreasing as the temperature is decreasing. With the temperature increasing, the vibration is dominant. So the influence of environments to the luminescence center could be enhanced with high temperature. ΔR between excited state and ground state at high temperature is increased, giving rise to the broad band emission. What is

more, one sharp line was detected in the spectra at 300K, which can also be found at 18 K. This sharp line could be related to R lines [44]. At 18 K the zero phonon line is separated by 50 cm^{-1} ; in the region of 760 to 790 nm, several phonon emission were investigated, there phonon lines was a result of strong electron-phonon coupling of the 3d ions.

(b) Excitation

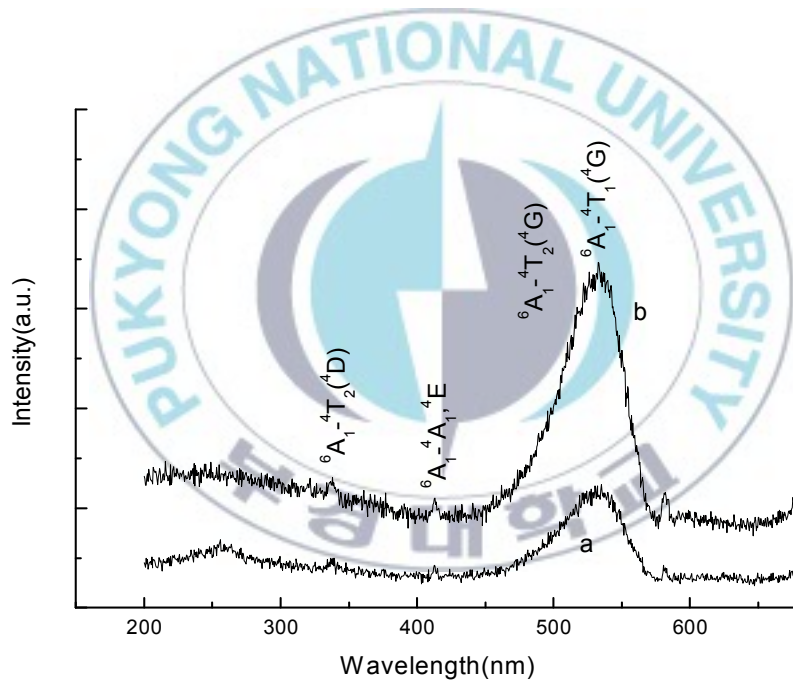
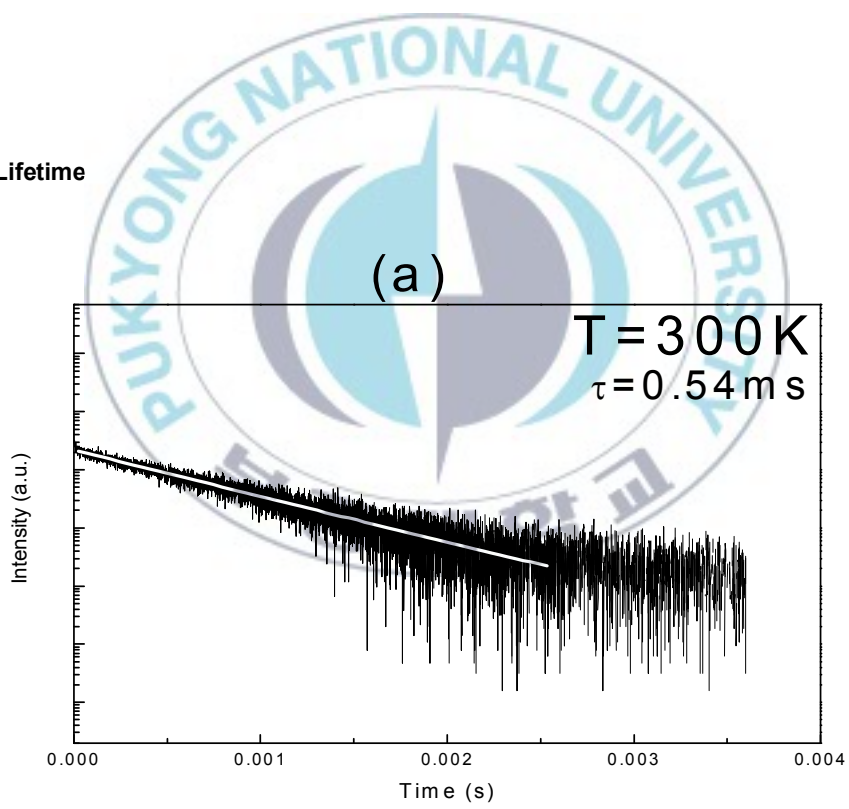


Fig. 4.12 Excitation spectra of Mn²⁺-LiBaF₃ monitoring at $\lambda_{Em}=750 \text{ nm}$ at room temperature. (a) LiBaF₃:Mn²⁺ 0.5mol%; (b) LiBaF₃:Mn²⁺ 0.05mol%.

The excitation spectra monitoring at $\lambda_{Em}=750 \text{ nm}$ was investigated

shown in the above figure. The excitation band centered at 532 nm comes to an account to absorption peaks center at 525 nm in the absorption spectra. The excitation spectrum extends a broad range of wavelength and is consistent with the diffuse reflectance spectra. The high-energy stronger band in the range 450–580 nm can be assigned to the mixture of absorption of defect and d-d transitions. The low-energy (400–450 nm) bands are attributed to the d–d transitions of Mn^{2+} ; the intensities of these bands are weaker because the corresponding transitions are spin-forbidden. The excitation band situated at about 340 nm can be attributed to the ${}^6A_1 \rightarrow {}^4T_2({}^4D)$ transition, whereas the excitation band situated at about 530 nm can be attributed to ${}^6A_1 \rightarrow {}^4T_1, {}^4T_2(4G)$ transitions; there are some weak narrow bandwidths at about 410 nm, which can be attributed to ${}^6A_1 \rightarrow {}^4A_1, {}^4E$ transitions. The 4A_1 and 4E levels have the same energy and are parallel to the ground level 6A_1 , so the absorption band corresponding to ${}^6A_1 \rightarrow {}^4A_1, {}^4E$ has a narrow bandwidth, lying at 410 nm, irrespective of the kind of host material. This band splits into more than one line when carefully investigated. The splitting is considered to reflect the reduction of the crystal field symmetry.

(c) Lifetime



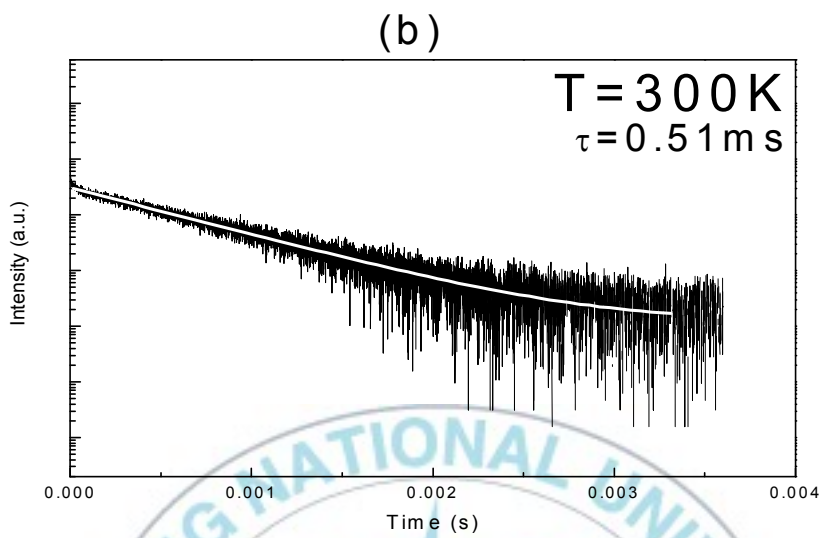
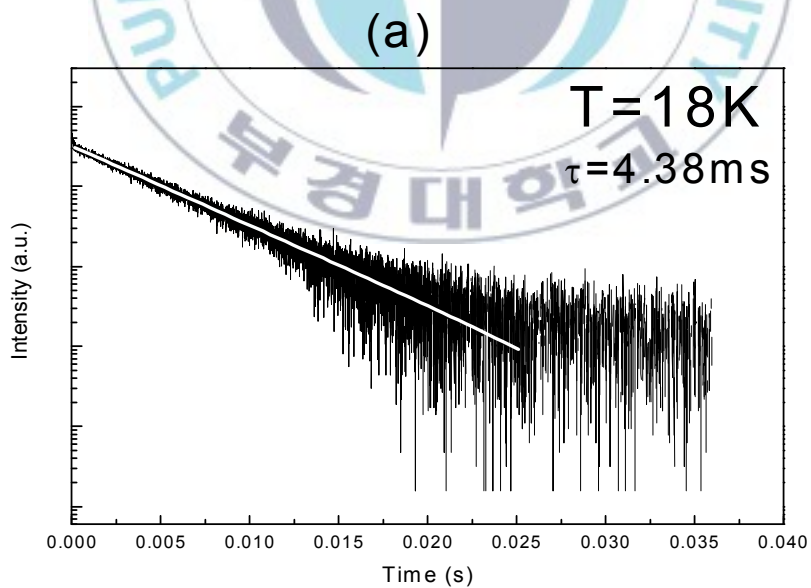


Fig. 4.13 Decay curves excited by 532 nm pulsed laser monitoring at 750 nm at 300 K, (a) LiBaF₃:Mn0.5mol%; (b) LiBaF₃:Mn0.05mol%.



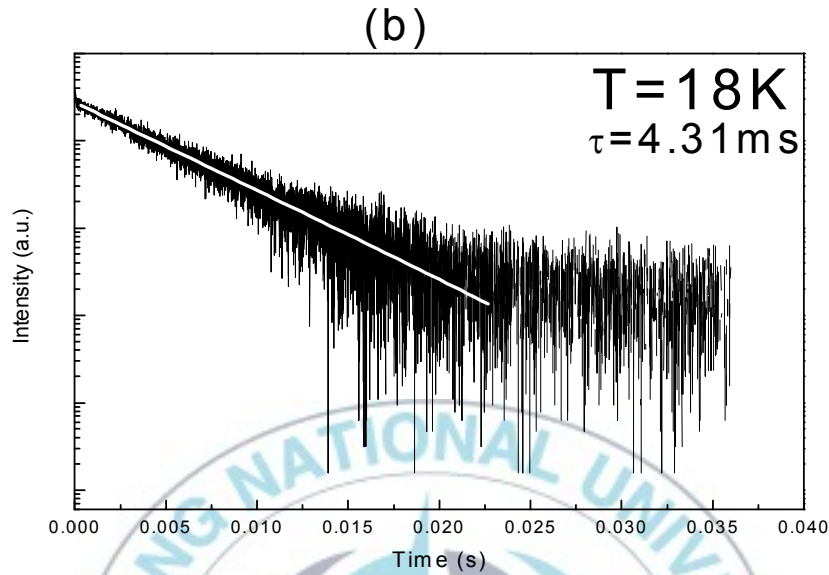


Fig. 4.14 Decay curves of LiBaF₃: Mn at 18 K; (a) LiBaF₃:Mn²⁺ 0.5mol% (b) LiBaF₃: Mn²⁺ 0.05mol%

The fluorescence lifetime measured at different temperatures decreases from about 4.3 ms at 18 K to about 0.5 ms at 300 K, the long lifetime at low temperature being the intrinsic lifetime of the emitting level. The reduction of lifetime with temperature shows the thermal quenching of this level (Figure 4.13; 4.14) while the decay stays always exponential. The lifetime is independent with the doping concentration. When the doping concentration is different, the lifetime is nearly the same.

5. Conclusion

The Mn-doped LiBaF_3 single crystals were prepared by the Czochralski method. The LiBaF_3 melted incongruently and the single crystal grew from a non-stoichiometric melt to avoid other phase precipitations. The different mole ratios of the LiF and BaF_2 powder influence the purity of the LiBaF_3 compounds greatly. The best mole ratio is 3:2. Also, the effect of two times calcinations can enhance the purity of the compounds. Having many times of experiment, we find that the initial temperature cooling rate should be lower than $0.5\text{ }^\circ\text{C/h}$ and a good initial part of the crystal is very important which requires the neck of the crystal should be long and small. Since the crucible is big without a platinum attemperator and the LiBaF_3 single crystal is grown from the non-stoichiometric melt, the pulling speed should be lower than 0.5 mm/h . Otherwise, there would be many cracks inside the crystal. Different rotation speeds yield the different temperature fields which also influence the optical properties of the LiBaF_3 single crystal.

Although the 3d-3d transition is parity forbidden, the selection rules were loosen by the exchange mechanism (spin-spin interaction) and a vibronic mechanism (coupling with odd lattice vibrations which partially destroy the inversion centre). The emission spectra of 3d-3d transition at 515 nm when Mn^{2+} is substituted into the Ba^{2+} site and 3d-3d transition at around 750 nm when Mn^{2+} is replacing the Li^+ site in the octahedral

symmetry are observed. These two broad band emissions of Mn^{2+} are helpful to analyze the crystallographic symmetry sites in the LiBaF_3 crystal. The intensity of emission spectra shows no big changes with different doping concentration of Mn^{2+} ions. The decay curves of Mn^{2+} can be well fitted by single exponential equation and the decay time is decreasing from 0.9ms at 18 K to 0.5ms at 300 K if Mn^{2+} is substituted into the Ba^{2+} site, while the decay time from 4.3 ms at 18 K to 0.5 ms at 300 K if Mn^{2+} replaces the Li^+ site. The temperature dependent decay curves show the thermal quenching of ${}^4\text{T}_1\text{-}{}^6\text{A}_1$ emission level. The zero-phonon line of the 3d-3d transition in two sites was observed. In Ba^{2+} site, ZPL appear with some phonon lines, which were investigated considering electronic phonon coupling, while in Li^+ site, ZPL were detected together with the other sharp electronic or vibrational lines which could be ascribed to the strong electron-phonon coupling of the 3d ions.

References

- [1] W. A. Sibley and N. Koumvakalis. *Physical Review B* **14(1)**, 35 (1976).
- [2] M. A. Losada, R. Alcala, P. J. Alonso, R. Cases, and V. M. Orera, *Radiation Effects Express*, **2**, 39 (1988).
- [3] P. L. Reeder, S.M. Bowyer, *IEEE Transactions on Nuclear Science*, **48**, 351 (2001).
- [4] C. M. Combes, P. Dorenbos, R. W. Hollander, C. W. E. van Eijk, *Nuclear Instruments and Methods in Physics Research Section A: Accelerators, Spectrometers, Detectors and Associated Equipment*, **A 416**, 364 (1998).
- [5] M. J. Knitel, P. Dorenbos, J. T. M. de Haas, C. W. E. van Eijk, *Nuclear Instruments and Methods in Physics Research Section A: Accelerators, Spectrometers, Detectors and Associated Equipment*, **374**, 197 (1996).
- [6] P.L. Reeder, S.M. Bowyer, *Journal of Radioanalytical and Nuclear Chemistry*, **248**, 707 (2001).
- [7] A.V. Gektin, *Journal of Luminescence*, **87**, 1283 (2000).
- [8] N. Shiran, V. Voronova, *Journal of Luminescence*, **87**, 561 (2000).
- [9] A.V. Gektin, N.V. Shiran, V.V. Voroncva, *IEEE Transactions on Nuclear Science*, **44**, 857 (1997).
- [10] E. Radzhabov, V. Otroshok, *Journal of Physics and Chemistry of Solids*, **56**, 1 (1995).
- [11] E. Radzhabov, P. Figura, *physica status solidi (b)*, **186**, 37 (1994).

- [12] Weber, M.J., Physical Review **157**, 262 (1967).
- [13] Lakowicz, J.R., "Principles of Fluorescence Spectroscopy". Third Edition. Springer, New York, (2006).
- [14] S. I. Klink, G. A. Hebbink, L. Grave, F. C. J. M. Van Veggel, D. N. Reinhoudt, L. H. Slooff, A. Polman, and J. W. Hofstraat, Journal of applied physics, **86**, 1181 (1999).
- [15] Valeur, B. "Molecular Fluorescence Principles and Applications", Wiley-VCH, Weinheim, Germany, (2002).
- [16] Kitai, A.H., "Solid State Luminescence: Theory, materials and devices", First Edition. Springer, New York, (1993).
- [17] So, P., and Dong, C.Y., "Fluorescence spectrophotometry", Encyclopedia of Life Science, Nature Publishing Group, (2002).
- [18] Brixner, L.H., Journal of Chemical Education, **57**, pp. 588-590 (1980).
- [19] Blasse, G. and Grabmaier, B.C., "Luminescent Materials". Springer Verlag, (1994).
- [20] S. Sugano, Y. Tanabe and H. Kamimura, "Multiplets of Transition-Metal Ions in Crystals", Academic Press, New York (1970).
- [21] Xinmin Zhang, Heping Zeng and Qiang Su, Journal of Alloys and Compounds, **441**, 259 (2007).
- [22] B. Henderson, and G. F. Imbusch, "Optical Spectroscopy of Inorganic Solids", Clarendon Press, Oxford, (1989).
- [23] S. L. Baldochi and J. Y. Gesland, Materials Research Bulletin, **27**, 891 (1992).

- [24] D'Ans-Lax, "Taschenbuch fur Chemiker und Physiker", edited by K. Schafer and C. Synowitz, Springer-Verlag (1970).
- [25] T. Yosida, H. Aoki, H. Takeuchi, M. Arakawa, and K. Horai, Journal of the Physical Society of Japan, **46**, 1661 (1979).
- [26] F. Rodriguez and M. Moreno. Journal of Chemical Physics, **84(2)**, 692 (1986).
- [27] A Neuhaus, H.G.Holz and H.D. Klein, zeitschrift fur physikalische chemie-international journal of research in physical chemistry & chemical physics, **53**, 163 (1967).
- [28] R. Lechebusch, A. Neuhaus and K. Recker, Journal of Crystal Growth, **16**, 10 (1972)
- [29] Liang Shi, "Crystal growth and excited-state dynamics of Eu²⁺ Luminescence in Eu-doped LiBaF₃ single crystals" thesis for the degree of master, Pukyong National University (2008).
- [30] S. L. Baldochi and J. Y. Gesland, Materials Research Bulletin, **27**, 891 (1992).
- [31] E. S. Kim, "Luminescence Properties of Er³⁺ ions doped in calcium Niobium Gallium Garnet Crystal", thesis for the degree of master, Pukyong National University (2008).
- [32] Warren, B.E., "X- Ray Diffraction", Dover Publications, New York, (1990).
- [33] Jingfang Zhou, Zhishen Wu, Zhijun Zhang, Weimin Liu, Hongxin Dang, Wear, **249**, 333 (2001).

- [34] B Henke, U Rogulis and S Schweizer, Journal of Physics: Condensed Matter, **18**, 1577 (2006).
- [35] P. Thiyagarajan, M. Kottaisamy, M.S. Ramachandra Rao, Scripta Materialia, **57**, 433 (2007).
- [36] L. Xiong, J. Shi, J. Gu, L. Li, W. Huang, J. Gao, M. Ruan, The Journal of Physical Chemistry B **109**, 731 (2005).
- [37] J. Ferguson, H.J. Guggenheim, Physical Review B **1**, 4223 (1970).
- [38] M.D. Shinn, J.C. Windschleif, D.K. Sardar, W.A. Sibley. Physical Review B **26**, 2371 (1982).
- [39] G. U Caldiño, Journal of Physics: Condensed Matter, **15**, 7127 (2003).
- [40] B Henderson, G.F. Imbusch, "Optical Spectroscopy of Inorganic Solids", Oxford University Press, UK (1989).
- [41] DIETRICH LANGER, SUMIAKI IBUKI, Physical review B **138**, A809, (1965).
- [42] Marcus True, "Fine structure in d-f and f -f transitions of Tm³⁺ and systematic investigation of 3d⁵ - 3d⁴4s absorption of Mn²⁺ doped fluorides", DISSERTATION, (2004).
- [43] M. Marsman, J. Andriessen, and C. W. E van Eijk, Physical review B **61**, 16477, (2000).
- [44] M. Mortier, J. Y. Gesland, B. Piriou, J. Y. Buzaré, M. Rousseau, Optical Materials **4**,115 (1994).

Acknowledgements

The accomplishment of this paper benefits from the enlightenment of my supervisor, Professor Hyo Jin Seo, whose inspiring insights, generous encouragements, and enthusiastic instructions have facilitated me much throughout my thesis writing. His penetrating and insightful comments afford me with inspiring source. He has been in constant concern about my paper, spared no pains to entertain my thesis draft. I would also like to extend my sincere thanks to Professor Jae Yong Je and Dr. Kyoung Hyuk Jang. Thanks to their instructive guidance and comprehensive education during the two years' schooling.

I would like to express my heartfelt gratitude to Prof. Yanlin Huang and Dr. Liang Shi. Without their consistent and illuminating instruction, this thesis could not have reached its present form.

Finally, my great gratitude also goes to those writers whose works I have perused and benefited greatly from without which the completion of the thesis would not have been possible.